Central exclusive diffractive production of the $\pi^+\pi^-$ continuum, scalar, and tensor resonances in pp and $p\bar{p}$ scattering within the tensor Pomeron approach

Piotr Lebiedowicz,[1,*] Otto Nachtmann,[2,†] and Antoni Szczurek[1,‡]

[1]*Institute of Nuclear Physics, Polish Academy of Sciences, Radzikowskiego 152,*
PL-31-342 Kraków, Poland
[2]*Institut für Theoretische Physik, Universität Heidelberg, Philosophenweg 16,*
D-69120 Heidelberg, Germany

We consider central exclusive diffractive dipion production in the reactions $pp \to pp\pi^+\pi^-$ and $p\bar{p} \to p\bar{p}\pi^+\pi^-$ at high energies. We include the dipion continuum, the dominant scalar $f_0(500)$, $f_0(980)$, and tensor $f_2(1270)$ resonances decaying into the $\pi^+\pi^-$ pairs. The calculation is based on a tensor Pomeron model and the amplitudes for the processes are formulated in terms of vertices respecting the standard crossing and charge-conjugation relations of quantum field theory. The formulas for the dipion continuum and tensor meson production are given here for the first time. The theoretical results are compared with existing STAR, CDF, CMS experimental data and predictions for planned or current experiments (ALICE, ATLAS) are presented. We show the influence of the experimental cuts on the integrated cross section and on various differential distributions for outgoing particles. Distributions in rapidities and transverse momenta of outgoing protons and pions as well as correlations in azimuthal angle between them are presented. We find that the relative contribution of the resonant $f_2(1270)$ and dipion continuum strongly depends on the cut on proton transverse momenta or four-momentum transfer squared $t_{1,2}$ which may explain some controversial observations made by different ISR experiments in the past. The cuts may play then the role of a $\pi\pi$ resonance filter. We suggest some experimental analyses to fix model parameters related to the Pomeron-Pomeron–f_2 coupling.

I. INTRODUCTION

The exclusive reaction $pp \to pp\pi^+\pi^-$ is one of the reactions being extensively studied by several experimental groups such as COMPASS [1–3], STAR [4,5], CDF [6,7], ALICE [8], ATLAS [9], and CMS [10,11]. It is commonly believed that at high energies the Pomeron-Pomeron fusion is the dominant mechanism of the exclusive two-pion production. In the past, two of us have formulated a simple Regge-inspired model of the two-pion continuum mediated by the double Pomeron/Reggeon exchanges with parameters fixed from phenomenological analyses of NN and πN scattering [12].[1] The number of free model parameters is then limited to a parameter of form factor describing off-shellness of the exchanged pion. The largest uncertainties in the model are due to the unknown off-shell pion form factor and the absorption corrections discussed recently in

[16]. Although this model gives correct order-of-magnitude cross sections, it is not able to describe details of differential distributions, in particular the distribution in dipion invariant mass where we observe a rich pattern of structures. Clearly such an approach does not include resonance contributions which interfere with the continuum. It is found that the pattern of visible structures depends on experiment but as we rather advocate on the cuts used in a particular experiment (usually these cuts are different for different experiments).

It has been known for a long time that the commonly used vector Pomeron has problems from a field-theory point of view. Taken literally, it gives opposite signs for pp and $p\bar{p}$ total cross sections. For a discussion of this point, see, for instance, chapter 6 of [17]. The argument is simple. Consider, first, a single photon, that is, a vector exchange between two electrons and between an electron and positron. The potentials and also the scattering amplitudes have opposite signs. For e^-e^-, the potential is repulsive; for e^-e^+, it is attractive. In complete analogy, a field-theoretical vector-Pomeron exchange gives opposite signs for the pp and $p\bar{p}$ scattering amplitudes. But this also implies opposite signs for the pp and $p\bar{p}$ total cross sections since these are proportional to the imaginary parts of the forward scattering amplitudes. A way out of this dilemma

---

*Piotr.Lebiedowicz@ifj.edu.pl
†O.Nachtmann@thphys.uni-heidelberg.de
‡Antoni.Szczurek@ifj.edu.pl
Also at University of Rzeszów, PL-35-959 Rzeszów, Poland.

[1]For another related work, see [13] where the exclusive reaction $pp \to pp\pi^+\pi^-$ constitutes an irreducible background to the scalar χ_{c0} meson production. These model studies were extended also to the $pp \to ppK^+K^-$ [14] and the $pp \to nn\pi^+\pi^+$ [15] processes.

was already shown in [17], where the Pomeron was described as a coherent superposition of exchanges with spin $2 + 4 + 6 + \cdots$. This same idea is realized in a very practical way in the tensor-Pomeron model formulated in [18]. In this model, Pomeron exchange can effectively be treated as the exchange of a rank-2 tensor. As we see easily from the analogy to the case of gravity, this gives the same sign for the potential and for the scattering amplitudes for pp and $p\bar{p}$. This is as it should be, since the Pomeron has charge conjugation $C = +1$. The corresponding couplings of the tensorial object to proton and pion were worked out. In Ref. [19], the model was applied to the production of several scalar and pseudoscalar mesons in the reaction $pp \to ppM$. A good description of the experimental distributions [20] was achieved at relatively low energy, although there Reggeon exchanges still play a very important role.[2] The resonant $(\rho^0 \to \pi^+\pi^-)$ and nonresonant (Drell-Söding) photon-Pomeron/Reggeon $\pi^+\pi^-$ production in pp collisions was studied in [22]. In [23], an extensive study of the photoproduction reaction $\gamma p \to \pi^+\pi^- p$ in the framework of the tensor-Pomeron model was presented.

In most of the experimental preliminary spectra of the $pp \to pp\pi^+\pi^-$ reaction at higher energies, a peak at $M_{\pi\pi} \sim 1270$ MeV is observed. One can expect that the peak is related to the production of the well known tensor isoscalar meson $f_2(1270)$ which decays with high probability into the $\pi^+\pi^-$ channel. In principle, contributions from the $f_0(1370)$, $f_0(1500)$ and $f_0(1710)$ mesons are not excluded. The $f_0(1500)$ and $f_0(1710)$ mesons are often considered as potential candidates for scalar states with dominant glueball content, and it is expected that in Pomeron-Pomeron fusion the glueball production could be prominently enhanced due to the gluonic nature of the Pomeron [24,25].

For a study of the resonance production observed in the $\pi^+\pi^-$ and K^+K^- mass spectra in the fixed target experiments at low energies, see Refs. [26–30]. There is evidence from the analysis of the decay modes of the scalar states observed, that the lightest scalar glueball manifests itself through the mixing with nearby $q\bar{q}$ states [30] and that the difference in the transverse momentum vectors between the two exchange particles (dP_t) can be used to select out known $q\bar{q}$ states from non-$q\bar{q}$ candidates.[3] In addition, the four-momentum transfer squared $|t|$ from one of the proton vertices for the resonances was determined. For the tensor $f_2(1270)$ and $f_2'(1525)$ states, their fractional distributions

show nonsingle exponential behavior; see Fig. 5 of [27]. It has been observed in [26] that the $\rho(770)$, $\phi(1020)$, $f_2(1270)$ and $f_2'(1525)$ resonances are visible more efficiently in the high $t = |t_1 + t_2|$ region ($t > 0.3$ GeV^2) and that at low t their signals are suppressed.

In the ISR experiments, see [32–34], the $\pi^+\pi^-$ invariant mass distribution shows an enhancement in the low-mass (S-wave) region and a very significant resonance structure. A clear $f_2(1270)$ signal has been observed at $\sqrt{s} = 62$ GeV [32] and a cross section $\sigma(pp \to ppf_2, f_2 \to \pi^+\pi^-)$ of $(8 \pm 1 \pm 3)$ μb was determined, where the four-momentum transfer squared is $|t| \geq 0.08$ GeV^2, the scattered protons have $x_{F,p} \geq 0.9$, and the pion c.m. system rapidity is limited to the region $|y_\pi| \geq 1.5$. However, this behavior is rather different from that observed in Ref. [35]. In our opinion, this is due to the different kinematic coverage of these two ISR experiments. The experiment [35] has been performed at $\sqrt{s} = 63$ GeV. Compared to [32], their analysis covered smaller four-momentum transfer squared $(0.01 \lesssim |t| \lesssim 0.06$ GeV$^2)$, $x_{F,p} \geq 0.95$, and the central rapidity region was more restricted. Moreover, their D-wave cross section shows an enhancement between 1.2 and 1.5 GeV, and the authors of [35] argued that the $f_2(1270)$ alone does not explain the behavior of the data and additional states are needed, e.g. a scalar at around 1400 MeV and tensor at $m = 1480 \pm 50$ MeV with $\Gamma = 150 \pm 50$ MeV. In Ref. [34], the cross section of central $\pi^+\pi^-$ production shows an enhancement in both the S and D waves near the mass of the $f_2(1270)$ and $f_0(1400)$. The D-wave mass spectrum was described with the $f_2(1270)$ resonant state and a broad background term. A cross section for exclusive $f_2(1270)$ meson production of 5.0 ± 0.7 μb (not including a systematic error, estimated to be 1.5 μb) was obtained.

On the theoretical side, the production of the tensor meson f_2 has not been considered so far in the literature, except in Ref. [36]. We note that in a recent work [37] the authors also consider the resonance production through the Pomeron-Pomeron fusion at the LHC but ignore the spin effects in the Pomeron-Pomeron-meson vertices. In the present paper, we consider both production of the two-pion continuum and of the $f_0(500)$, $f_0(980)$, and $f_2(1270)$ resonances in the $\pi^+\pi^-$ channel, consistent within the tensor-Pomeron model. This model allows us also to calculate interference effects. We consider the tensor-tensor-tensor coupling in a Lagrangian formalism and present a list of possible couplings. The specificities of the different couplings are discussed, also in the context of experimental results. We discuss a first qualitative attempt to "reproduce" the experimentally observed behaviors of the two-pion spectra obtained in the $pp \to pp\pi^+\pi^-$ reaction and discuss consequences of experimental cuts on the observed spectra. The calculations presented in Sec. V were done with a FORTRAN code using the VEGAS routine [38].

---

[2]The role of secondary Reggeons in central pseudoscalar meson production was discussed also in Ref. [21].

[3]It has been observed in Ref. [31] that all the undisputed $q\bar{q}$ states (i.e. η, η', $f_1(1285)$, etc.) are suppressed as $dP_t \to 0$, whereas the glueball candidates, e.g. $f_0(1500)$, survive. As can be seen there, $\rho^0(770)$, $f_2(1270)$ and $f_2'(1525)$ have larger dP_t and their cross sections peak at $\phi_{pp} = \pi$, i.e. the outgoing protons are on opposite sides of the beam, in contrast to the "enigmatic" $f_0(980)$, $f_0(1500)$ and $f_0(1710)$ states.

II. EXCLUSIVE TWO-PION PRODUCTION

We study central exclusive production of $\pi^+\pi^-$ in proton-proton collisions at high energies

$$p(p_a, \lambda_a) + p(p_b, \lambda_b)$$
$$\rightarrow p(p_1, \lambda_1) + \pi^+(p_3) + \pi^-(p_4) + p(p_2, \lambda_2), \quad (2.1)$$

where $p_{a,b}$, $p_{1,2}$ and $\lambda_{a,b}$, $\lambda_{1,2} \in \{+1/2, -1/2\}$ denote the four-momenta and helicities of the protons, and $p_{3,4}$ denote the four-momenta of the charged pions, respectively.

The full amplitude of $\pi^+\pi^-$ production is a sum of the continuum amplitude and the amplitudes through the s-channel resonances:

$$\mathcal{M}_{pp \rightarrow pp\pi^+\pi^-} = \mathcal{M}^{\pi\pi\text{-continuum}}_{pp \rightarrow pp\pi^+\pi^-} + \mathcal{M}^{\pi\pi\text{-resonances}}_{pp \rightarrow pp\pi^+\pi^-}. \quad (2.2)$$

This amplitude for central exclusive $\pi^+\pi^-$ production is believed to be given by the fusion of two exchange objects. The generic "Born level" diagram is shown in Fig. 1, where we label the exchange objects by their charge conjugation numbers $C_1, C_2 \in \{+1, -1\}$. At high energies the exchange objects to be considered are the photon γ, the Pomeron $\mathbb{P}$, the Odderon $\mathbb{O}$, and the Reggeons $\mathbb{R} = f_{2\mathbb{R}}, a_{2\mathbb{R}}, \omega_{\mathbb{R}}, \rho_{\mathbb{R}}$. Their charge conjugation numbers and G parities are listed in Table I.

In calculating the amplitude (2.2) from the diagram Fig. 1, a sum over all combinations of exchanges, $(C_1, C_2) = (1, 1), (-1, -1), (1, -1), (-1, 1)$, has to be taken:

$$\mathcal{M}_{pp \rightarrow pp\pi^+\pi^-} = \mathcal{M}^{(1,1)} + \mathcal{M}^{(-1,-1)} + \mathcal{M}^{(1,-1)} + \mathcal{M}^{(-1,1)}. \quad (2.3)$$

Note that the (1,1) and $(-1, -1)$ contributions will produce a $\pi^+\pi^-$ state with charge conjugation $C = +1$. The $(1, -1)$ and $(-1, 1)$ contributions will produce a $\pi^+\pi^-$ state with $C = -1$. This implies that the $\mathcal{M}^{(C_1,C_2)}$ amplitudes have the following properties under exchange of the π^+ and π^- momenta, keeping all other kinematic variables, indicated by the dots, fixed:
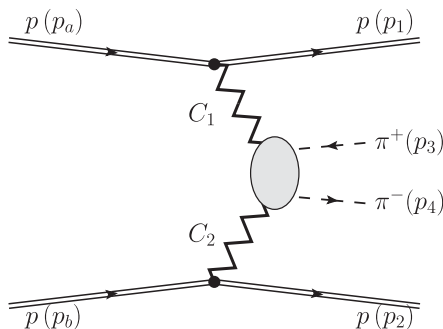

FIG. 1. Generic "Born level" diagram for central exclusive $\pi^+\pi^-$ production in proton-proton collisions.

TABLE I. Charge conjugation and G-parity quantum numbers of exchange objects for resonance and continuum production.

Exchange object	C	G
$\mathbb{P}$	1	1
$f_{2\mathbb{R}}$	1	1
$a_{2\mathbb{R}}$	1	-1
γ	-1	
$\mathbb{O}$	-1	-1
$\omega_{\mathbb{R}}$	-1	-1
$\rho_{\mathbb{R}}$	-1	1

$$\mathcal{M}^{(1,1)}(\dots, p_3, p_4) = \mathcal{M}^{(1,1)}(\dots, p_4, p_3),$$
$$\mathcal{M}^{(-1,-1)}(\dots, p_3, p_4) = \mathcal{M}^{(-1,-1)}(\dots, p_4, p_3),$$
$$\mathcal{M}^{(1,-1)}(\dots, p_3, p_4) = -\mathcal{M}^{(1,-1)}(\dots, p_4, p_3),$$
$$\mathcal{M}^{(-1,1)}(\dots, p_3, p_4) = -\mathcal{M}^{(-1,1)}(\dots, p_4, p_3). \quad (2.4)$$

The interference of the amplitudes $\mathcal{M}^{(1,1)} + \mathcal{M}^{(-1,-1)}$ with $\mathcal{M}^{(1,-1)} + \mathcal{M}^{(-1,1)}$ will lead to asymmetries under exchange of the π^+ and π^- momenta. Such asymmetries can, for instance, be studied in the rest frame of the $\pi^+\pi^-$ pair using a convenient coordinate system like the Collins-Soper frame [39]. For a discussion of various reference frames, see for instance [23,40]. Asymmetries may be quite interesting from an experimental point of view since they could allow us to measure small contributions in the amplitude which would be hard to detect otherwise. Some details related to the asymmetries are given in Appendix B.

III. TWO-PION CONTINUUM PRODUCTION

The generic diagrams for the exclusive two-pion continuum production are shown in Fig. 2. Taking into account the G parity of -1 for the pions, we get the following combinations (C_1, C_2) of exchanges which can contribute[4]:

$$(C_1, C_2) = (1, 1): \ (\mathbb{P} + f_{2\mathbb{R}}, \mathbb{P} + f_{2\mathbb{R}}); \quad (3.1)$$

$$(C_1, C_2) = (-1, -1): \ (\rho_{\mathbb{R}} + \gamma, \rho_{\mathbb{R}} + \gamma); \quad (3.2)$$

$$(C_1, C_2) = (1, -1): \ (\mathbb{P} + f_{2\mathbb{R}}, \rho_{\mathbb{R}} + \gamma); \quad (3.3)$$

$$(C_1, C_2) = (-1, 1): \ (\rho_{\mathbb{R}} + \gamma, \mathbb{P} + f_{2\mathbb{R}}). \quad (3.4)$$

Note that for the cases involving the photon γ in (3.2) to (3.4), one also has to take into account the diagrams involving the corresponding contact terms; see [23].

From the above list of exchange contributions, we have already treated $(\mathbb{P} + f_{2\mathbb{R}}, \gamma)$ and $(\gamma, \mathbb{P} + f_{2\mathbb{R}})$ in [22]. At

---

[4]Note that G parity invariance forbids the vertices $a_{2\mathbb{R}}\pi\pi$, $\omega_{\mathbb{R}}\pi\pi$, $\mathbb{O}\pi\pi$; see Table I. Thus, the exchanges of $a_{2\mathbb{R}}, \omega_R, \mathbb{O}$ cannot contribute to the dipion continuum.
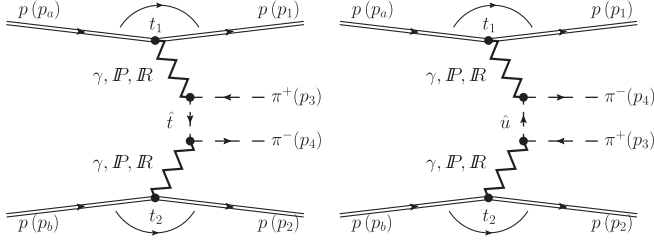
FIG. 2. The Born diagrams for the double Pomeron/Reggeon and photon mediated central exclusive continuum $\pi^+\pi^-$ production in proton-proton collisions.

high energies, the contributions involving $\rho_{\mathbb{R}}$ exchanges are expected to be small since $\rho_{\mathbb{R}}$ is a secondary Reggeon and its coupling to the proton is small; see e.g. (3.61),

(3.62) of [18]. The (γ, γ) contribution is higher order in α_{em}. Thus, we are left with the contribution $(\mathbb{P} + f_{2\mathbb{R}}, \mathbb{P} + f_{2\mathbb{R}})$, (3.1), which we shall treat now.

The amplitude for the corresponding diagrams in Fig. 2 can be written as the following sum[5]:

$$\mathcal{M}^{\pi\pi\text{-continuum}}_{pp \to pp\pi^+\pi^-} = \mathcal{M}^{(\mathbb{P}\mathbb{P} \to \pi^+\pi^-)} + \mathcal{M}^{(\mathbb{P}f_{2\mathbb{R}} \to \pi^+\pi^-)}$$
$$+ \mathcal{M}^{(f_{2\mathbb{R}}\mathbb{P} \to \pi^+\pi^-)} + \mathcal{M}^{(f_{2\mathbb{R}}f_{2\mathbb{R}} \to \pi^+\pi^-)}. \quad (3.5)$$

The $\mathbb{P}\mathbb{P}$-exchange amplitude can be written as

$$\mathcal{M}^{(\mathbb{P}\mathbb{P} \to \pi^+\pi^-)} = \mathcal{M}^{(\hat{t})}_{\lambda_a\lambda_b \to \lambda_1\lambda_2\pi^+\pi^-} + \mathcal{M}^{(\hat{u})}_{\lambda_a\lambda_b \to \lambda_1\lambda_2\pi^+\pi^-}, \quad (3.6)$$

where

$$\mathcal{M}^{(\hat{t})}_{\lambda_a\lambda_b \to \lambda_1\lambda_2\pi^+\pi^-} = (-i)\bar{u}(p_1,\lambda_1)i\Gamma^{(\mathbb{P}pp)}_{\mu_1\nu_1}(p_1,p_a)u(p_a,\lambda_a)i\Delta^{(\mathbb{P})\mu_1\nu_1,\alpha_1\beta_1}(s_{13},t_1)i\Gamma^{(\mathbb{P}\pi\pi)}_{\alpha_1\beta_1}(p_t,-p_3)i\Delta^{(\pi)}(p_t)$$
$$\times i\Gamma^{(\mathbb{P}\pi\pi)}_{\alpha_2\beta_2}(p_4,p_t)i\Delta^{(\mathbb{P})\alpha_2\beta_2,\mu_2\nu_2}(s_{24},t_2)\bar{u}(p_2,\lambda_2)i\Gamma^{(\mathbb{P}pp)}_{\mu_2\nu_2}(p_2,p_b)u(p_b,\lambda_b), \quad (3.7)$$

$$\mathcal{M}^{(\hat{u})}_{\lambda_a\lambda_b \to \lambda_1\lambda_2\pi^+\pi^-} = (-i)\bar{u}(p_1,\lambda_1)i\Gamma^{(\mathbb{P}pp)}_{\mu_1\nu_1}(p_1,p_a)u(p_a,\lambda_a)i\Delta^{(\mathbb{P})\mu_1\nu_1,\alpha_1\beta_1}(s_{14},t_1)i\Gamma^{(\mathbb{P}\pi\pi)}_{\alpha_1\beta_1}(p_4,p_u)i\Delta^{(\pi)}(p_u)$$
$$\times i\Gamma^{(\mathbb{P}\pi\pi)}_{\alpha_2\beta_2}(p_u,-p_3)i\Delta^{(\mathbb{P})\alpha_2\beta_2,\mu_2\nu_2}(s_{23},t_2)\bar{u}(p_2,\lambda_2)i\Gamma^{(\mathbb{P}pp)}_{\mu_2\nu_2}(p_2,p_b)u(p_b,\lambda_b), \quad (3.8)$$

where $p_t = p_a - p_1 - p_3$ and $p_u = p_4 - p_a + p_1$, $s_{ij} = (p_i + p_j)^2$. The kinematic variables for reaction (2.1) are

$$s = (p_a + p_b)^2 = (p_1 + p_2 + p_3 + p_4)^2,$$
$$s_{34} = M^2_{\pi\pi} = (p_3 + p_4)^2,$$
$$t_1 = q_1^2, \qquad t_2 = q_2^2, \qquad q_1 = p_a - p_1,$$
$$q_2 = p_b - p_2. \quad (3.9)$$

Here $\Delta^{(\mathbb{P})}$ and $\Gamma^{(\mathbb{P}pp)}$ denote the effective propagator and proton vertex function, respectively, for the tensorial Pomeron. For the explicit expressions, see Sec. III of [18]. The normal pion propagator is $i\Delta^{(\pi)}(k) = i/(k^2 - m^2_\pi)$. In a similar way, the $\mathbb{P}f_{2\mathbb{R}}$, $f_{2\mathbb{R}}\mathbb{P}$ and $f_{2\mathbb{R}}f_{2\mathbb{R}}$ amplitudes can be written.

The propagator of the tensor-Pomeron exchange is written as (see Eq. (3.10) of [18]):

$$i\Delta^{(\mathbb{P})}_{\mu\nu,\kappa\lambda}(s,t) = \frac{1}{4s}\left(g_{\mu\kappa}g_{\nu\lambda} + g_{\mu\lambda}g_{\nu\kappa} - \frac{1}{2}g_{\mu\nu}g_{\kappa\lambda}\right)(-is\alpha'_{\mathbb{P}})^{\alpha_{\mathbb{P}}(t)-1}$$

$$(3.10)$$

and fulfils the following relations:

$$\Delta^{(\mathbb{P})}_{\mu\nu,\kappa\lambda}(s,t) = \Delta^{(\mathbb{P})}_{\nu\mu,\kappa\lambda}(s,t) = \Delta^{(\mathbb{P})}_{\mu\nu,\lambda\kappa}(s,t) = \Delta^{(\mathbb{P})}_{\kappa\lambda,\mu\nu}(s,t),$$
$$g^{\mu\nu}\Delta^{(\mathbb{P})}_{\mu\nu,\kappa\lambda}(s,t) = 0, \qquad g^{\kappa\lambda}\Delta^{(\mathbb{P})}_{\mu\nu,\kappa\lambda}(s,t) = 0. \quad (3.11)$$

For the $f_{2\mathbb{R}}$ Reggeon exchange, a similar form of the effective propagator and the $f_{2\mathbb{R}}pp$ and $f_{2\mathbb{R}}\pi\pi$ effective vertices is assumed; see (3.12) and (3.49), (3.53) of [18]. Here the Pomeron and Reggeon trajectories $\alpha_i(t)$, where $i = \mathbb{P}, \mathbb{R}$, are assumed to be of standard linear forms; see e.g. [41],

$$\alpha_{\mathbb{P}}(t) = \alpha_{\mathbb{P}}(0) + \alpha'_{\mathbb{P}}t, \qquad \alpha_{\mathbb{P}}(0) = 1.0808,$$
$$\alpha'_{\mathbb{P}} = 0.25 \text{ GeV}^{-2}, \quad (3.12)$$

$$\alpha_{\mathbb{R}}(t) = \alpha_{\mathbb{R}}(0) + \alpha'_{\mathbb{R}}t, \qquad \alpha_{\mathbb{R}}(0) = 0.5475,$$
$$\alpha'_{\mathbb{R}} = 0.9 \text{ GeV}^{-2}. \quad (3.13)$$

The corresponding coupling of tensor Pomeron to protons (antiprotons), including a vertex form factor, is written as (see Eq. (3.43) of [18])

---

[5]We emphasize, that not only the leading Pomeron exchanges contribute to the dipion system with the isospin $I = 0$ and $C = +1$ but also the $\mathbb{P}f_{2\mathbb{R}}$, $f_{2\mathbb{R}}\mathbb{P}$, $f_{2\mathbb{R}}f_{2\mathbb{R}}$, $\rho_{\mathbb{R}}\rho_{\mathbb{R}}$ exchanges and due to their non-negligible interference effects with the leading $\mathbb{P}\mathbb{P}$ term the subleading $f_{2\mathbb{R}}$ exchanges must be included explicitly in our calculations.

$$i\Gamma_{\mu\nu}^{(\mathbb{P}pp)}(p',p) = i\Gamma_{\mu\nu}^{(\mathbb{P}\bar{p}\bar{p})}(p',p)$$

$$= -i3\beta_{\mathbb{P}NN}F_1((p'-p)^2)\left\{\frac{1}{2}[\gamma_\mu(p'+p)_\nu\right.$$

$$\left.+\gamma_\nu(p'+p)_\mu] - \frac{1}{4}g_{\mu\nu}(p\!\!\!/'+p\!\!\!/)\right\}, \quad (3.14)$$

where $\beta_{\mathbb{P}NN} = 1.87$ GeV^{-1}. Starting with the $\mathbb{P}\pi\pi$ coupling Lagrangian (see Eq. (7.3) of [18]), we have the following $\mathbb{P}\pi\pi$ vertex (see Eq. (3.45) of [18]):

$$i\Gamma_{\mu\nu}^{(\mathbb{P}\pi\pi)}(k',k) = -i2\beta_{\mathbb{P}\pi\pi}\left[(k'+k)_\mu(k'+k)_\nu\right.$$

$$\left.-\frac{1}{4}g_{\mu\nu}(k'+k)^2\right]F_M((k'-k)^2), \quad (3.15)$$

where $\beta_{\mathbb{P}\pi\pi} = 1.76$ GeV^{-1} gives proper phenomenological normalization. The form factors taking into account that the hadrons are extended objects (see Sec. 3.2 of [41]) are chosen as

$$F_1(t) = \frac{4m_p^2 - 2.79t}{(4m_p^2 - t)(1 - t/m_D^2)^2}, \quad F_M(t) = \frac{1}{1 - t/\Lambda_0^2}, \quad (3.16)$$

where m_p is the proton mass and $m_D^2 = 0.71$ GeV^2 is the dipole mass squared and $\Lambda_0^2 = 0.5$ GeV^2; see Eq. (3.34) of [18]. Alternatively, instead of the product of the form factors $F_1(t)F_M(t)$ where the two factors are attached to the relevant vertices [see Eqs. (3.14) and (3.15)], we can take single form factors $F_{\pi N}^{(\mathbb{P}/\mathbb{R})}(t)$ in the exponential form where

the Pomeron/Reggeon slope parameters have been estimated from a fit to the πp elastic scattering data; see Eq. (2.11) and Fig. 3 of [16].

The amplitudes (3.9) and (3.12) must be "corrected" for the off-shellness of the intermediate pions. The form of the off-shell pion form factor is unknown in particular at higher values of p_t^2 or p_u^2. The form factors are normalized to unity at the on-shell point $\hat{F}_\pi(m_\pi^2) = 1$ and parametrized here in two ways:

$$\hat{F}_\pi(k^2) = \exp\left(\frac{k^2 - m_\pi^2}{\Lambda_{\text{off},E}^2}\right), \quad (3.17)$$

$$\hat{F}_\pi(k^2) = \frac{\Lambda_{\text{off},M}^2 - m_\pi^2}{\Lambda_{\text{off},M}^2 - k^2}, \quad (3.18)$$

where $\Lambda_{\text{off},E}^2$ or $\Lambda_{\text{off},M}^2$ could be adjusted to experimental data. It was shown in Fig. 9 of [16] that the monopole form (3.18) is supported by the preliminary CDF results [7] particularly at higher values of two-pion invariant mass, $M_{\pi\pi} > 1.5$ GeV. Thus, in the numerical calculations below (see Sec. V), we used the monopole form of the off-shell pion form factors (with the exception of the right panel of Fig. 12).

In the high-energy small-angle approximation, we have

$$\bar{u}(p',\lambda')\gamma_\mu(p'+p)_\nu u(p,\lambda) \to (p'+p)_\mu(p'+p)_\nu\delta_{\lambda'\lambda}, \quad (3.19)$$

and we can write the leading terms of the amplitudes for the $pp \to pp\pi^+\pi^-$ process as

$$\mathcal{M}_{\lambda_a\lambda_b\to\lambda_1\lambda_2\pi^+\pi^-}^{(\hat{t})} \simeq 3\beta_{\mathbb{P}NN}2(p_1+p_a)_{\mu_1}(p_1+p_a)_{\nu_1}\delta_{\lambda_1\lambda_a}F_1(t_1)F_M(t_1)$$

$$\times 2\beta_{\mathbb{P}\pi\pi}(p_t-p_3)^{\mu_1}(p_t-p_3)^{\nu_1}\frac{1}{4s_{13}}(-is_{13}\alpha_{\mathbb{P}}')^{\alpha_{\mathbb{P}}(t_1)-1}\frac{[\hat{F}_\pi(p_t^2)]^2}{p_t^2-m_\pi^2}$$

$$\times 2\beta_{\mathbb{P}\pi\pi}(p_4+p_t)^{\mu_2}(p_4+p_t)^{\nu_2}\frac{1}{4s_{24}}(-is_{24}\alpha_{\mathbb{P}}')^{\alpha_{\mathbb{P}}(t_2)-1}$$

$$\times 3\beta_{\mathbb{P}NN}2(p_2+p_b)_{\mu_2}(p_2+p_b)_{\nu_2}\delta_{\lambda_2\lambda_b}F_1(t_2)F_M(t_2), \quad (3.20)$$

$$\mathcal{M}_{\lambda_a\lambda_b\to\lambda_1\lambda_2\pi^+\pi^-}^{(\hat{u})} \simeq 3\beta_{\mathbb{P}NN}2(p_1+p_a)_{\mu_1}(p_1+p_a)_{\nu_1}\delta_{\lambda_1\lambda_a}F_1(t_1)F_M(t_1)$$

$$\times 2\beta_{\mathbb{P}\pi\pi}(p_4+p_u)^{\mu_1}(p_4+p_u)^{\nu_1}\frac{1}{4s_{14}}(-is_{14}\alpha_{\mathbb{P}}')^{\alpha_{\mathbb{P}}(t_1)-1}\frac{[\hat{F}_\pi(p_u^2)]^2}{p_u^2-m_\pi^2}$$

$$\times 2\beta_{\mathbb{P}\pi\pi}(p_u-p_3)^{\mu_2}(p_u-p_3)^{\nu_2}\frac{1}{4s_{23}}(-is_{23}\alpha_{\mathbb{P}}')^{\alpha_{\mathbb{P}}(t_2)-1}$$

$$\times 3\beta_{\mathbb{P}NN}2(p_2+p_b)_{\mu_2}(p_2+p_b)_{\nu_2}\delta_{\lambda_2\lambda_b}F_1(t_2)F_M(t_2). \quad (3.21)$$

Now, we consider the vector Pomeron exchange model. We have the following ansatz for the $\mathbb{P}_V\pi^-\pi^-$ vertex omitting the form factors ($M_0 \equiv 1$ GeV)

TABLE II. Resonances and (C_1, C_2) production modes.

$I^G J^{PC}$	Resonance	Production (C_1, C_2)
0^+0^{++}	$f_0(500)$	$(\mathbb{P} + f_{2\mathbb{R}}, \mathbb{P} + f_{2\mathbb{R}}), (a_{2\mathbb{R}}, a_{2\mathbb{R}}),$
	$f_0(980)$	$(\mathbb{O} + \omega_{\mathbb{R}} + \gamma, \mathbb{O} + \omega_{\mathbb{R}} + \gamma), (\rho_{\mathbb{R}}, \rho_{\mathbb{R}}),$
	$f_0(1370)$	$(\gamma, \rho_{\mathbb{R}}), (\rho_{\mathbb{R}}, \gamma)$
	$f_0(1500)$	
	$f_0(1710)$	
1^+1^{--}	$\rho(770)$	$(\gamma + \rho_{\mathbb{R}}, \mathbb{P} + f_{2\mathbb{R}}), (\mathbb{P} + f_{2\mathbb{R}}, \gamma + \rho_{\mathbb{R}}),$
	$\rho(1450)$	$(\mathbb{O} + \omega_{\mathbb{R}}, a_{2\mathbb{R}}), (a_{2\mathbb{R}}, \mathbb{O} + \omega_{\mathbb{R}})$
	$\rho(1700)$	
0^+2^{++}	$f_2(1270)$	$(\mathbb{P} + f_{2\mathbb{R}}, \mathbb{P} + f_{2\mathbb{R}}), (a_{2\mathbb{R}}, a_{2\mathbb{R}}),$
	$f_2'(1525)$	$(\mathbb{O} + \omega_{\mathbb{R}} + \gamma, \mathbb{O} + \omega_{\mathbb{R}} + \gamma), (\rho_{\mathbb{R}}, \rho_{\mathbb{R}}),$
	$f_2(1950)$	$(\gamma, \rho_{\mathbb{R}}), (\rho_{\mathbb{R}}, \gamma)$
1^+3^{--}	$\rho_3(1690)$	$(\gamma + \rho_{\mathbb{R}}, \mathbb{P} + f_{2\mathbb{R}}), (\mathbb{P} + f_{2\mathbb{R}}, \gamma + \rho_{\mathbb{R}}),$
		$(\mathbb{O} + \omega_{\mathbb{R}}, a_{2\mathbb{R}}), (a_{2\mathbb{R}}, \mathbb{O} + \omega_{\mathbb{R}})$
0^+4^{++}	$f_4(2050)$	$(\mathbb{P} + f_{2\mathbb{R}}, \mathbb{P} + f_{2\mathbb{R}}), (a_{2\mathbb{R}}, a_{2\mathbb{R}}),$
		$(\mathbb{O} + \omega_{\mathbb{R}} + \gamma, \mathbb{O} + \omega_{\mathbb{R}} + \gamma), (\rho_{\mathbb{R}}, \rho_{\mathbb{R}}),$
		$(\gamma, \rho_{\mathbb{R}}), (\rho_{\mathbb{R}}, \gamma)$

$$i\Gamma_\mu^{(\mathbb{P}_V \pi^- \pi^-)}(k', k) = -i2\beta_{\mathbb{P}\pi\pi} M_0 (k' + k)_\mu. \quad (3.22)$$

From isospin and charge-conjugation invariance we should have

$$i\Gamma_\mu^{(\mathbb{P}_V \pi^+ \pi^+)}(k', k) = i\Gamma_\mu^{(\mathbb{P}_V \pi^- \pi^-)}(k', k). \quad (3.23)$$

But the crossing relations require

$$i\Gamma_\mu^{(\mathbb{P}_V \pi^+ \pi^+)}(k', k) = i\Gamma_\mu^{(\mathbb{P}_V \pi^- \pi^-)}(-k, -k'). \quad (3.24)$$

And from (3.22) we get

$$i\Gamma_\mu^{(\mathbb{P}_V \pi^- \pi^-)}(-k, -k') = -i\Gamma_\mu^{(\mathbb{P}_V \pi^- \pi^-)}(k', k). \quad (3.25)$$

Clearly, (3.23) and (3.24) plus (3.25) would lead to $i\Gamma_\mu^{(\mathbb{P}_V \pi\pi)}(k', k) \equiv 0$. This is another manifestation that the $\mathbb{P}_V \pi\pi$ coupling for a vector Pomeron has basic problems; see also the discussion in Sec. 6.1 of [18].

IV. DIPION RESONANT PRODUCTION

In this section, we consider the production of s-channel resonances which decay to $\pi^+\pi^-$

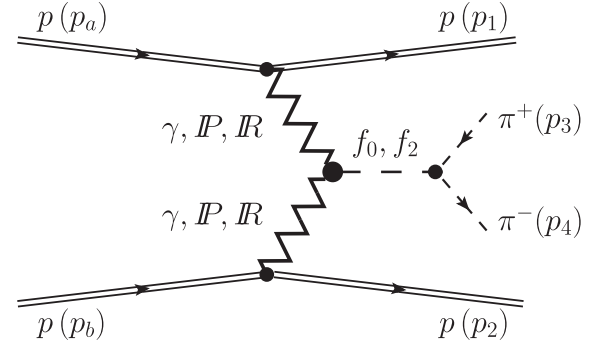$$p + p \rightarrow p + (\text{resonance} \rightarrow \pi^+\pi^-) + p. \quad (4.1)$$

FIG. 3. The Born diagram for the double Pomeron/Reggeon and photon mediated central exclusive $I^G J^{PC} = 0^+0^{++}$ and 0^+2^{++} resonances production and their subsequent decays into $\pi^+\pi^-$ in proton-proton collisions.

The resonances which should be taken into account here and their production modes via (C_1, C_2) fusion are listed in Table II.

The production of $\rho(770)$ and $\rho(1450)$ was already treated in [22]. Here we shall discuss the production of the f_0 and f_2 resonances; see Fig. 3. We shall concentrate on the contributions from $(C_1, C_2) = (\mathbb{P} + f_{2\mathbb{R}}, \mathbb{P} + f_{2\mathbb{R}})$. We can justify this as follows. The contributions involving the Odderon (if it exists at all), the $a_{2\mathbb{R}}$ and the $\rho_{\mathbb{R}}$ should be small due to small couplings of these objects to the proton. The secondary Reggeons $a_{2\mathbb{R}}, \omega_{\mathbb{R}}, \rho_{\mathbb{R}}$ should give small contributions at high energies. We shall neglect contributions involving the photon γ in the following. These are expected to become important only for very small values of $|t_1|$ and/or $|t_2|$. Thus we are left with $(\mathbb{P} + f_{2\mathbb{R}}, \mathbb{P} + f_{2\mathbb{R}})$ where $(\mathbb{P}, \mathbb{P})$ fusion is the leading term and $(\mathbb{P}, f_{2\mathbb{R}})$ plus $(f_{2\mathbb{R}}, \mathbb{P})$ is the first nonleading term due to Reggeons at high energies.

The amplitude for exclusive resonant $\pi^+\pi^-$ production, given by the diagram shown in Fig. 3, can be written as

$$\mathcal{M}_{pp \rightarrow pp\pi^+\pi^-}^{\pi\pi\text{-resonances}} = \mathcal{M}_{\lambda_a\lambda_b \rightarrow \lambda_1\lambda_2\pi^+\pi^-}^{(\mathbb{P}\mathbb{P} \rightarrow f_0 \rightarrow \pi^+\pi^-)} + \mathcal{M}_{\lambda_a\lambda_b \rightarrow \lambda_1\lambda_2\pi^+\pi^-}^{(\mathbb{P}\mathbb{P} \rightarrow f_2 \rightarrow \pi^+\pi^-)}. \quad (4.2)$$

A. $I^G J^{PC} = 0^+0^{++}$

For a scalar meson, $J^{PC} = 0^{++}$, the amplitude for $\mathbb{P}\mathbb{P}$ fusion can be written as

$$\mathcal{M}_{\lambda_a\lambda_b \rightarrow \lambda_1\lambda_2\pi^+\pi^-}^{(\mathbb{P}\mathbb{P} \rightarrow f_0 \rightarrow \pi^+\pi^-)} = (-i)\bar{u}(p_1, \lambda_1) i\Gamma_{\mu_1\nu_1}^{(\mathbb{P}pp)}(p_1, p_a) u(p_a, \lambda_a) i\Delta^{(\mathbb{P})\mu_1\nu_1,\alpha_1\beta_1}(s_1, t_1)$$

$$\times i\Gamma_{\alpha_1\beta_1,\alpha_2\beta_2}^{(\mathbb{P}\mathbb{P}f_0)}(q_1, q_2) i\Delta^{(f_0)}(p_{34}) i\Gamma^{(f_0\pi\pi)}(p_{34})$$

$$\times i\Delta^{(\mathbb{P})\alpha_2\beta_2,\mu_2\nu_2}(s_2, t_2) \bar{u}(p_2, \lambda_2) i\Gamma_{\mu_2\nu_2}^{(\mathbb{P}pp)}(p_2, p_b) u(p_b, \lambda_b), \quad (4.3)$$

where $s_1 = (p_a + q_2)^2 = (p_1 + p_{34})^2$, $s_2 = (p_b + q_1)^2 = (p_2 + p_{34})^2$, and $p_{34} = p_3 + p_4$. The effective Lagrangians and the vertices for $\mathbb{P}\mathbb{P}$ fusion into the f_0 meson are discussed in Appendix A of [19]. As was shown there the tensorial $\mathbb{P}\mathbb{P}f_0$ vertex corresponds to the sum of two lowest values of (l, S), that is $(l, S) = (0, 0)$ and $(2, 2)$ with the corresponding coupling parameters $g'_{\mathbb{P}\mathbb{P}M}$ and $g''_{\mathbb{P}\mathbb{P}M}$, respectively. The vertex, including a form factor, reads then as follows ($p_{34} = q_1 + q_2$):

$$i\Gamma^{(\mathbb{P}\mathbb{P}f_0)}_{\mu\nu,\kappa\lambda}(q_1,q_2)$$
$$= (i\Gamma'^{(\mathbb{P}\mathbb{P}f_0)}_{\mu\nu,\kappa\lambda}|_{\text{bare}} + i\Gamma''^{(\mathbb{P}\mathbb{P}f_0)}_{\mu\nu,\kappa\lambda}(q_1,q_2)|_{\text{bare}})\tilde{F}^{(\mathbb{P}\mathbb{P}f_0)}(q_1^2,q_2^2,p_{34}^2);$$

$$(4.4)$$

see (A.21) of [19]. Unfortunately, the Pomeron-Pomeron-meson form factor is not well known as it is due to nonperturbative effects related to the internal structure of the respective meson. In practical calculations, we take the factorized form for the $\mathbb{P}\mathbb{P}f_0$ form factor,

$$\tilde{F}^{(\mathbb{P}\mathbb{P}f_0)}(q_1^2,q_2^2,p_{34}^2) = F_M(q_1^2)F_M(q_2^2)F^{(\mathbb{P}\mathbb{P}f_0)}(p_{34}^2), \quad (4.5)$$

normalized to $\tilde{F}^{(\mathbb{P}\mathbb{P}f_0)}(0, 0, m_{f_0}^2) = 1$. We will further set

$$F^{(\mathbb{P}\mathbb{P}f_0)}(p_{34}^2) = \exp\left(\frac{-(p_{34}^2 - m_{f_0}^2)^2}{\Lambda_{f_0}^4}\right), \quad \Lambda_{f_0} = 1 \, \text{GeV}. \quad (4.6)$$

The scalar-meson propagator is taken as

$$i\Delta^{(f_0)}(p_{34}) = \frac{i}{p_{34}^2 - m_{f_0}^2 + im_{f_0}\Gamma_{f_0}(p_{34}^2)}, \quad (4.7)$$

where the running (energy-dependent) width is parametrized as

$$\Gamma_{f_0}(p_{34}^2) = \Gamma_{f_0}\left(\frac{p_{34}^2 - 4m_\pi^2}{m_{f_0}^2 - 4m_\pi^2}\right)^{1/2}\theta(p_{34}^2 - 4m_\pi^2). \quad (4.8)$$

For the $f_0\pi\pi$ vertex, we have ($M_0 \equiv 1$ GeV)

$$i\Gamma^{(f_0\pi\pi)}(p_{34}) = ig_{f_0\pi\pi}M_0F^{(f_0\pi\pi)}(p_{34}^2), \quad (4.9)$$

where $g_{f_0\pi\pi}$ is related to the partial decay width of the f_0 meson (for an "on-shell" f_0 state $p_{34}^2 = m_{f_0}^2$)

$$\Gamma(f_0 \to \pi\pi) = 3\Gamma(f_0 \to \pi^0\pi^0) = \frac{3}{2}\Gamma(f_0 \to \pi^+\pi^-)$$
$$= \frac{3}{2}\frac{M_0^2}{16\pi m_{f_0}}|g_{f_0\pi\pi}|^2\left(1 - \frac{4m_\pi^2}{m_{f_0}^2}\right)^{1/2}. \quad (4.10)$$

We also assume that $F^{(f_0\pi\pi)}(p_{34}^2) = F^{(\mathbb{P}\mathbb{P}f_0)}(p_{34}^2)$; see Eq. (4.6).

In the high-energy small-angle approximation, we can write, setting $p_{34}^2 = s_{34}$,

$$\mathcal{M}^{(\mathbb{P}\mathbb{P} \to f_0 \to \pi^+\pi^-)}_{\lambda_a\lambda_b \to \lambda_1\lambda_2\pi^+\pi^-} \simeq 3\beta_{\mathbb{P}NN}2(p_1 + p_a)^{\mu_1}(p_1 + p_a)^{\nu_1}\delta_{\lambda_1\lambda_a}F_1(t_1)\frac{1}{4s_1}(-is_1\alpha'_\mathbb{P})^{\alpha_\mathbb{P}(t_1)-1}$$

$$\times \left[g'_{\mathbb{P}\mathbb{P}f_0}M_0\left(g_{\mu_1\mu_2}g_{\nu_1\nu_2} + g_{\mu_1\nu_2}g_{\nu_1\mu_2} - \frac{1}{2}g_{\mu_1\nu_1}g_{\mu_2\nu_2}\right)\right.$$

$$+ \frac{g''_{\mathbb{P}\mathbb{P}f_0}}{2M_0}(q_{1\mu_2}q_{2\mu_1}g_{\nu_1\nu_2} + q_{1\mu_2}q_{2\nu_1}g_{\mu_1\nu_2} + q_{1\nu_2}q_{2\mu_1}g_{\nu_1\mu_2} + q_{1\nu_2}q_{2\nu_1}g_{\mu_1\mu_2} - 2(q_1q_2)(g_{\mu_1\mu_2}g_{\nu_1\nu_2} + g_{\nu_1\mu_2}g_{\mu_1\nu_2}))\right]$$

$$\times \frac{g_{f_0\pi\pi}M_0}{s_{34} - m_{f_0}^2 + im_{f_0}\Gamma_{f_0}(s_{34})}\tilde{F}^{(\mathbb{P}\mathbb{P}f_0)}(t_1, t_2, s_{34})F^{(f_0\pi\pi)}(s_{34})$$

$$\times \frac{1}{4s_2}(-is_2\alpha'_\mathbb{P})^{\alpha_\mathbb{P}(t_2)-1}3\beta_{\mathbb{P}NN}2(p_2 + p_b)^{\mu_2}(p_2 + p_b)^{\nu_2}\delta_{\lambda_2\lambda_b}F_1(t_2). \quad (4.11)$$

From [42] we have for the mass and width of the $f_0(500)$ and $f_0(980)$ mesons

$$m_{f_0(500)} = 400\text{–}550 \text{ MeV}, \qquad \Gamma_{f_0(500)} = 400\text{–}700 \text{ MeV},$$
$$(4.12)$$

$$m_{f_0(980)} = 990 \pm 20 \text{ MeV}, \qquad \Gamma_{f_0(980)} = 40\text{–}100 \text{ MeV}.$$
$$(4.13)$$

We get, assuming $\Gamma(f_0 \to \pi\pi)/\Gamma_{f_0} = 100\%$, $m_{f_0(500)} = 600 \text{MeV}, \Gamma_{f_0(500)} = 500 \text{MeV}, m_{f_0(980)} = 980 \text{MeV}, \Gamma_{f_0(980)} = 70 \text{MeV}$, and assuming $g_{f_0\pi\pi} > 0$

$$g_{f_0(500)\pi\pi} = 3.37,$$
$$g_{f_0(980)\pi\pi} = 1.55. \quad (4.14)$$

B. $I^G J^{PC} = 0^+2^{++}$

The production of a tensor meson as $f_2 \equiv f_2(1270)$ is more complicated to treat. The amplitude for the $\pi\pi$ production through the s-channel f_2-meson exchange can be written as

$$
\begin{aligned}
\mathcal{M}^{(\mathbb{P}\mathbb{P}\to f_2\to\pi^+\pi^-)}_{\lambda_a\lambda_b\to\lambda_1\lambda_2\pi^+\pi^-} = {}& (-i)\bar{u}(p_1,\lambda_1)i\Gamma^{(\mathbb{P}pp)}_{\mu_1\nu_1}(p_1,p_a)u(p_a,\lambda_a)i\Delta^{(\mathbb{P})\mu_1\nu_1,\alpha_1\beta_1}(s_1,t_1) \\
& \times i\Gamma^{(\mathbb{P}\mathbb{P}f_2)}_{\alpha_1\beta_1,\alpha_2\beta_2,\rho\sigma}(q_1,q_2)i\Delta^{(f_2)\rho\sigma,\alpha\beta}(p_{34})i\Gamma^{(f_2\pi\pi)}_{\alpha\beta}(p_3,p_4) \\
& \times i\Delta^{(\mathbb{P})\alpha_2\beta_2,\mu_2\nu_2}(s_2,t_2)\bar{u}(p_2,\lambda_2)i\Gamma^{(\mathbb{P}pp)}_{\mu_2\nu_2}(p_2,p_b)u(p_b,\lambda_b).
\end{aligned}
\tag{4.15}
$$

The Pomeron-Pomeron–f_2 coupling is the most complicated element of our amplitudes. We have considered all possible tensorial structures for the coupling (see Appendix A). Then, the $\mathbb{P}\mathbb{P}f_2$ vertex can be written as

$$
i\Gamma^{(\mathbb{P}\mathbb{P}f_2)}_{\mu\nu,\kappa\lambda,\rho\sigma}(q_1,q_2) = \left(i\Gamma^{(\mathbb{P}\mathbb{P}f_2)(1)}_{\mu\nu,\kappa\lambda,\rho\sigma}\Big|_{\mathrm{bare}} + \sum_{j=2}^{7} i\Gamma^{(\mathbb{P}\mathbb{P}f_2)(j)}_{\mu\nu,\kappa\lambda,\rho\sigma}(q_1,q_2)\Big|_{\mathrm{bare}}\right)\tilde{F}^{(\mathbb{P}\mathbb{P}f_2)}(q_1^2,q_2^2,p_{34}^2).
\tag{4.16}
$$

Here $p_{34} = q_1 + q_2$ and $\tilde{F}^{(\mathbb{P}\mathbb{P}f_2)}$ is a form factor for which we make a factorized ansatz

$$
\tilde{F}^{(\mathbb{P}\mathbb{P}f_2)}(q_1^2,q_2^2,p_{34}^2) = F_M(q_1^2)F_M(q_2^2)F^{(\mathbb{P}\mathbb{P}f_2)}(p_{34}^2).
\tag{4.17}
$$

A possible choice for the $i\Gamma^{(\mathbb{P}\mathbb{P}f_2)(j)}_{\mu\nu,\kappa\lambda,\rho\sigma}\big|_{\mathrm{bare}}$ terms $j = 1,\ldots,7$ is given in Appendix A. We are taking here the same form factor for each vertex with index j ($j = 1,\ldots,7$). In principle, we could take a different form factor for each vertex.

Here, for qualitative calculations only, one may use the tensor-meson propagator with the simple Breit-Wigner form

$$
\begin{aligned}
i\Delta^{(f_2)}_{\mu\nu,\kappa\lambda}(p_{34}) = {}& \frac{i}{p_{34}^2 - m_{f_2}^2 + im_{f_2}\Gamma_{f_2}} \\
& \times \left[\frac{1}{2}(\hat{g}_{\mu\kappa}\hat{g}_{\nu\lambda} + \hat{g}_{\mu\lambda}\hat{g}_{\nu\kappa}) - \frac{1}{3}\hat{g}_{\mu\nu}\hat{g}_{\kappa\lambda}\right],
\end{aligned}
\tag{4.18}
$$

where $\hat{g}_{\mu\nu} = -g_{\mu\nu} + p_{34\mu}p_{34\nu}/p_{34}^2$. In (4.18), Γ_{f_2} is the total decay width of the $f_2(1270)$ resonance and m_{f_2} its mass. The propagator (4.18) fulfils the following relations:

$$
\Delta^{(f_2)}_{\mu\nu,\kappa\lambda}(p_{34}) = \Delta^{(f_2)}_{\nu\mu,\kappa\lambda}(p_{34}) = \Delta^{(f_2)}_{\mu\nu,\lambda\kappa}(p_{34}) = \Delta^{(f_2)}_{\kappa\lambda,\mu\nu}(p_{34}),
\tag{4.19}
$$

$$
g^{\mu\nu}\Delta^{(f_2)}_{\mu\nu,\kappa\lambda}(p_{34}) = 0, \qquad g^{\kappa\lambda}\Delta^{(f_2)}_{\mu\nu,\kappa\lambda}(p_{34}) = 0.
\tag{4.20}
$$

The $f_2\pi\pi$ vertex is written as (see Sec. 5.1 and Eqs. (3.37), (3.38) of [18])

$$
\begin{aligned}
i\Gamma^{(f_2\pi\pi)}_{\mu\nu}(p_3,p_4) = {}& -i\frac{g_{f_2\pi\pi}}{2M_0}\Bigg[(p_3-p_4)_\mu(p_3-p_4)_\nu \\
& -\frac{1}{4}g_{\mu\nu}(p_3-p_4)^2\Bigg]F^{(f_2\pi\pi)}(p_{34}^2),
\end{aligned}
\tag{4.21}
$$

where $g_{f_2\pi\pi} = 9.26$ was obtained from the corresponding partial decay width; see (5.6)–(5.9) of [18]. We assume that

$$
\begin{aligned}
F^{(f_2\pi\pi)}(p_{34}^2) = F^{(\mathbb{P}\mathbb{P}f_2)}(p_{34}^2) = {}& \exp\left(\frac{-(p_{34}^2-m_{f_2}^2)^2}{\Lambda_{f_2}^4}\right), \\
& \Lambda_{f_2} = 1\ \mathrm{GeV}.
\end{aligned}
\tag{4.22}
$$

In the high-energy small-angle approximation, we can write, setting $p_{34}^2 = s_{34}$,

$$
\begin{aligned}
\mathcal{M}^{(\mathbb{P}\mathbb{P}\to f_2\to\pi^+\pi^-)}_{\lambda_a\lambda_b\to\lambda_1\lambda_2\pi^+\pi^-} \simeq {}& -3\beta_{\mathbb{P}NN}2(p_1+p_a)^{\mu_1}(p_1+p_a)^{\nu_1}\delta_{\lambda_1\lambda_a}F_1(t_1)\frac{1}{4s_1}(-is_1\alpha_{\mathbb{P}}')^{\alpha_{\mathbb{P}}(t_1)-1} \\
& \times \Gamma^{(\mathbb{P}\mathbb{P}f_2)}_{\mu_1\nu_1,\mu_2\nu_2,\rho\sigma}(q_1,q_2)\Delta^{(f_2)\rho\sigma,\alpha\beta}(p_{34})\frac{g_{f_2\pi\pi}}{2M_0}(p_3-p_4)_\alpha(p_3-p_4)_\beta F^{(f_2\pi\pi)}(s_{34}) \\
& \times \frac{1}{4s_2}(-is_2\alpha_{\mathbb{P}}')^{\alpha_{\mathbb{P}}(t_2)-1}3\beta_{\mathbb{P}NN}2(p_2+p_b)^{\mu_2}(p_2+p_b)^{\nu_2}\delta_{\lambda_2\lambda_b}F_1(t_2).
\end{aligned}
\tag{4.23}
$$

This general form is, however, not easy to use as we do not know the normalization of each of the seven $\mathbb{P}\mathbb{P}f_2$ couplings. In principle, the parameters could be fitted to experimental data. However, we are not yet ready to perform such an analysis at present. Instead, we will consider properties of each of the individual terms separately.

The production of the f_2 via $\mathbb{P}f_{2\mathbb{R}}$, $f_{2\mathbb{R}}\mathbb{P}$, and $f_{2\mathbb{R}}f_{2\mathbb{R}}$ fusion can be treated in a completely analogous way to the $\mathbb{P}\mathbb{P}$ fusion. But this would introduce further unknown parameters. Therefore, we neglect in our present study the above terms which are nonleading anyway at high energies.

V. PRELIMINARY RESULTS FOR PRESENT AND FUTURE EXPERIMENTS

In this section, we show some preliminary results of our calculations, including the two-pion continuum and the $\rho(770)$, $f_0(500)$, $f_0(980)$ and $f_2(1270)$ resonances which are known to decay into two pions [42]. We start from a discussion of some dependences for the central exclusive production of the $f_2(1270)$ meson at $\sqrt{s} = 200$ GeV and $|\eta_\pi| < 1$. In Fig. 4, we present different differential observables in transferred four-momentum squared t_1 or t_2 between the initial and final protons, in proton $p_{t,p}$ and pion $p_{t,\pi}$ transverse momenta as well as in the so-called
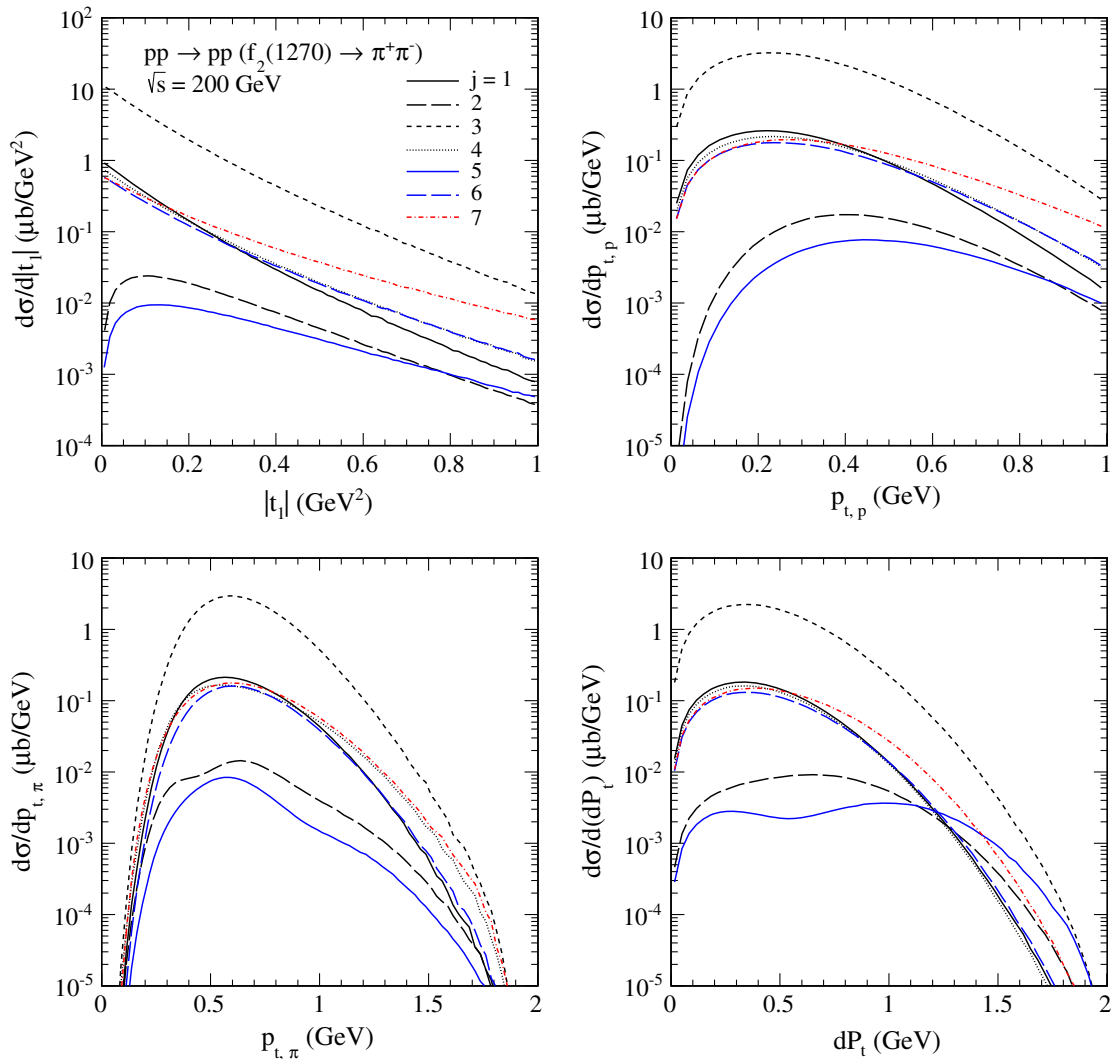

FIG. 4. The differential cross sections for the central exclusive production of the $f_2(1270)$ meson by the fusion of two tensor Pomerons at $\sqrt{s} = 200$ GeV and $|\eta_\pi| < 1$. We show the individual contributions of the different couplings: $j = 1$ (the black solid line), $j = 2$ (the black long-dashed line), $j = 3$ (the black dashed line), $j = 4$ (the black dotted line), $j = 5$ (the blue solid line), $j = 6$ (the blue long-dashed line), and $j = 7$ (the red dot-dashed line). For illustration, the results have been obtained with coupling constants $g_{\mathbb{P}\mathbb{P}f_2}^{(j)} = 1.0$. No absorption effects were included here.
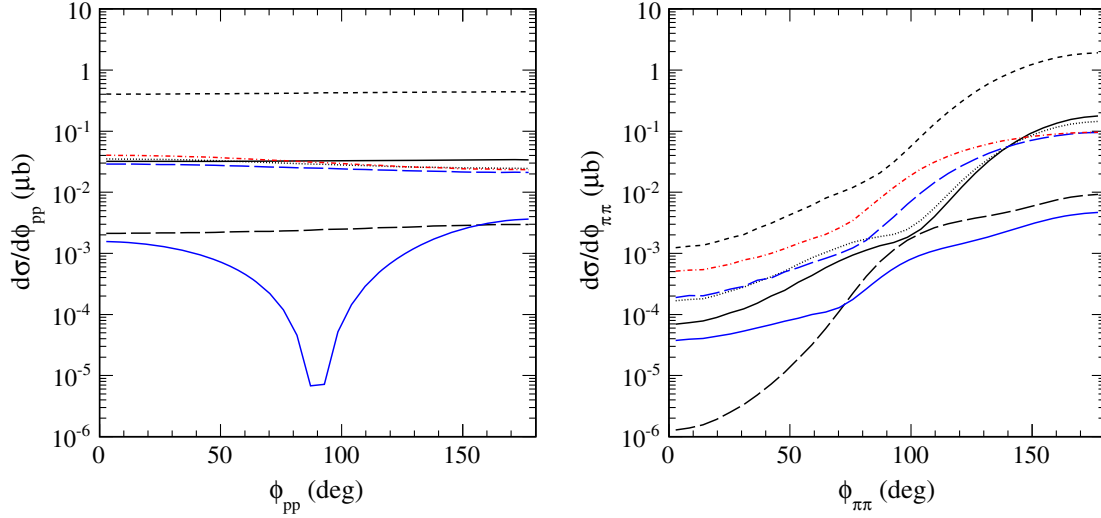
FIG. 5.   The distributions in azimuthal angle between the outgoing protons (left panel) and between the outgoing pions (right panel) for $\sqrt{s} = 200$ GeV and $|\eta_\pi| < 1$. The meaning of the lines is the same as in Fig. 4. No absorption effects were included here.

"glueball-filter variable" defined by the difference of the transverse momentum vectors $dP_t = |\boldsymbol{dP_t}|$ with $\boldsymbol{dP_t} = \boldsymbol{q_{t,1}} - \boldsymbol{q_{t,2}} = \boldsymbol{p_{t,2}} - \boldsymbol{p_{t,1}}$. We show results for the individual j coupling terms (see Appendix A). The predictions differ considerably which could be checked experimentally. We find that only in two cases ($j = 2$ and 5) does the cross section $d\sigma/d|t|$ vanish when $|t| \to 0$. Another possibility is that two different amplitudes could interfere so as to cancel exactly for $|t|$ going to zero but no longer cancel for larger $|t|$, although this seems rather improbable.

The distributions in azimuthal angle between the outgoing protons, ϕ_{pp}, and outgoing pions, $\phi_{\pi\pi}$, for

the central exclusive production of the $f_2(1270)$ meson at $\sqrt{s} = 200$ GeV and $|\eta_\pi| < 1$ are shown in Fig. 5 separately for different couplings. Only one of the seven couplings ($j = 5$) gives a minimum at $\phi_{pp} = \pi/2$. The shapes of the distributions in $\phi_{\pi\pi}$ are rather similar.

Different experiments reported results which seem contradictory [4,6]. Some of them [5,6] observed an appearance of the $f_2(1270)$ resonance and some not [4]. We think that this fact can be related to different coverage in t_1 and t_2 of the different experiments. Therefore, before showing any other results we wish to explore the t_1 and t_2 dependences. Two examples of
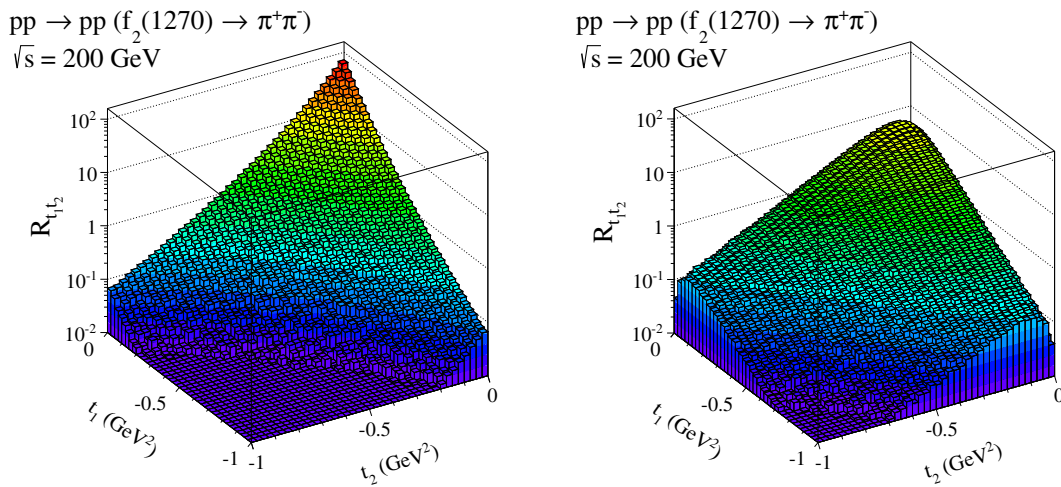

FIG. 6.   The distributions in (t_1, t_2) space for the central exclusive production of the $f_2(1270)$ meson via fusion of two tensor Pomerons at $\sqrt{s} = 200$ GeV and $|\eta_\pi| < 1$. Plotted is the ratio $R_{t_1 t_2} = \frac{d^2\sigma}{dt_1 dt_2} / \int dt_1 dt_2 \frac{d^2\sigma}{dt_1 dt_2}$. We show as examples the results for the $j = 1$ (left panel) and $j = 2$ (right panel) couplings. No absorption effects were included here.
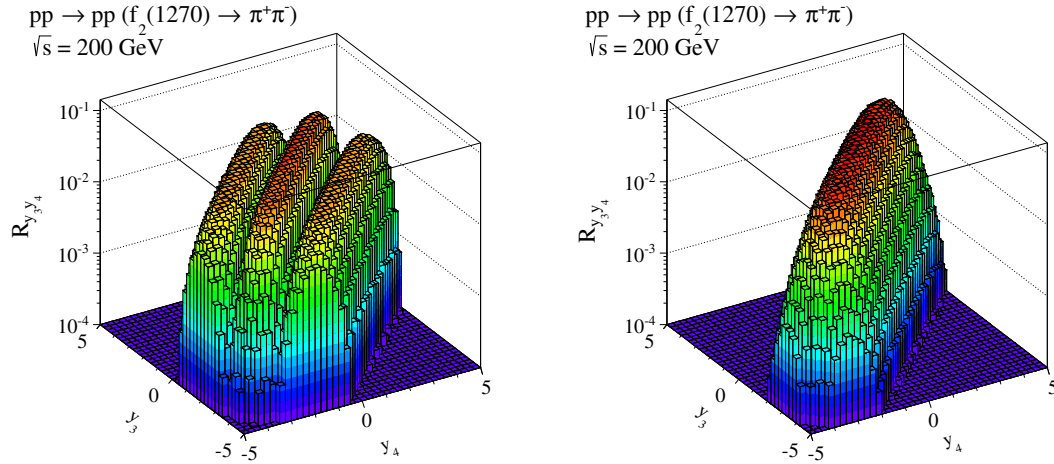
FIG. 7. The distributions in (y_3, y_4) space for the central exclusive production of the $f_2(1270)$ meson via fusion of two tensor Pomerons at $\sqrt{s} = 200$ GeV. Plotted is the ratio $R_{y_3 y_4} = \frac{d^2\sigma}{dy_3 dy_4} / \int dy_3 dy_4 \frac{d^2\sigma}{dy_3 dy_4}$. We show the results for the $j = 1$ (left panel) and $j = 2$ (right panel) couplings. No absorption effects were included here.
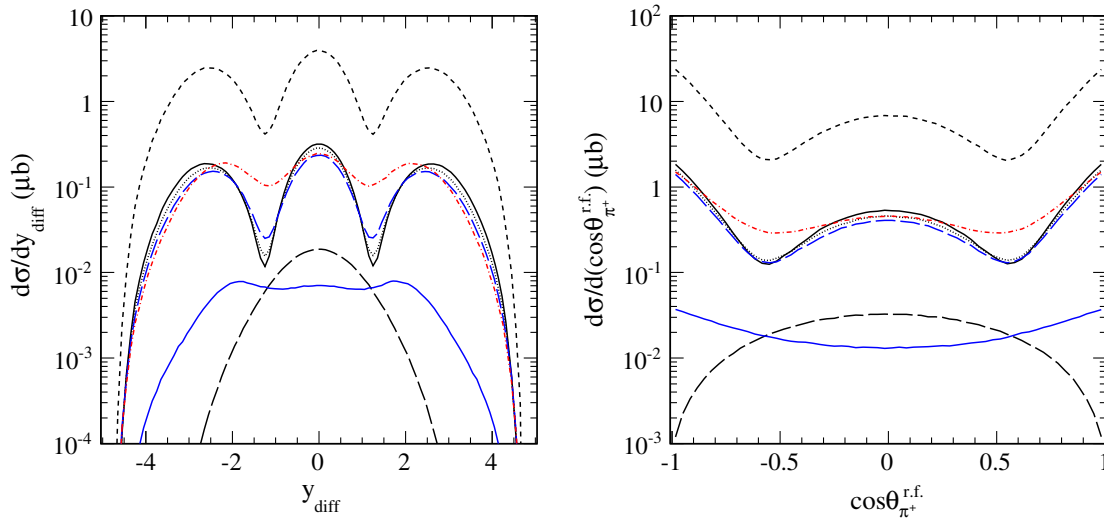

FIG. 8. The distributions in $y_{diff} = y_3 - y_4$ (the left panel) and in $\cos\theta_{\pi^+}^{r.f.}$ (the right panel). The meaning of the lines is the same as in Fig. 4 for $\sqrt{s} = 200$ GeV but here the calculation was done for a broader range of rapidities of both charged pions, $|y_\pi| < 5$. No absorption effects were included here.

the correlation between t_1 and t_2 for different Pomeron-Pomeron–f_2 couplings are displayed in Fig. 6. The general character of the distributions is rather different. While for $j = 1$ coupling we observe an enhancement of the cross section when $t_1 \to 0$ or $t_2 \to 0$, in the case of $j = 2$ coupling we observe a suppression of the cross section when $t_1 \to 0$ or $t_2 \to 0$.

The correlation in rapidity of the pions is displayed in Fig. 7 for two Pomeron-Pomeron–f_2 couplings. A very good one-dimensional observable which can be used for the comparison of the couplings under discussion could be the differential cross section $d\sigma/dy_{diff}$, where

$y_{diff} = y_3 - y_4$. We show the corresponding distribution in Fig. 8 (the left panel). In the right panel, we show the angular distribution of the π^+ meson, $\cos\theta_{\pi^+}^{r.f.}$, where $\theta_{\pi^+}^{r.f.}$ is the polar angle of the π^+ meson with respect to the beam axis in the $\pi^+\pi^-$ rest frame. One can observe correlations between the left and right panel. The minima in the left panel correspond to minima in the right panel. This is related to the kinematical transformation between y_{diff} and $\cos\theta_{\pi^+}^{r.f.}$.

In the present preliminary analysis, we wish to understand whether one can approximately describe the
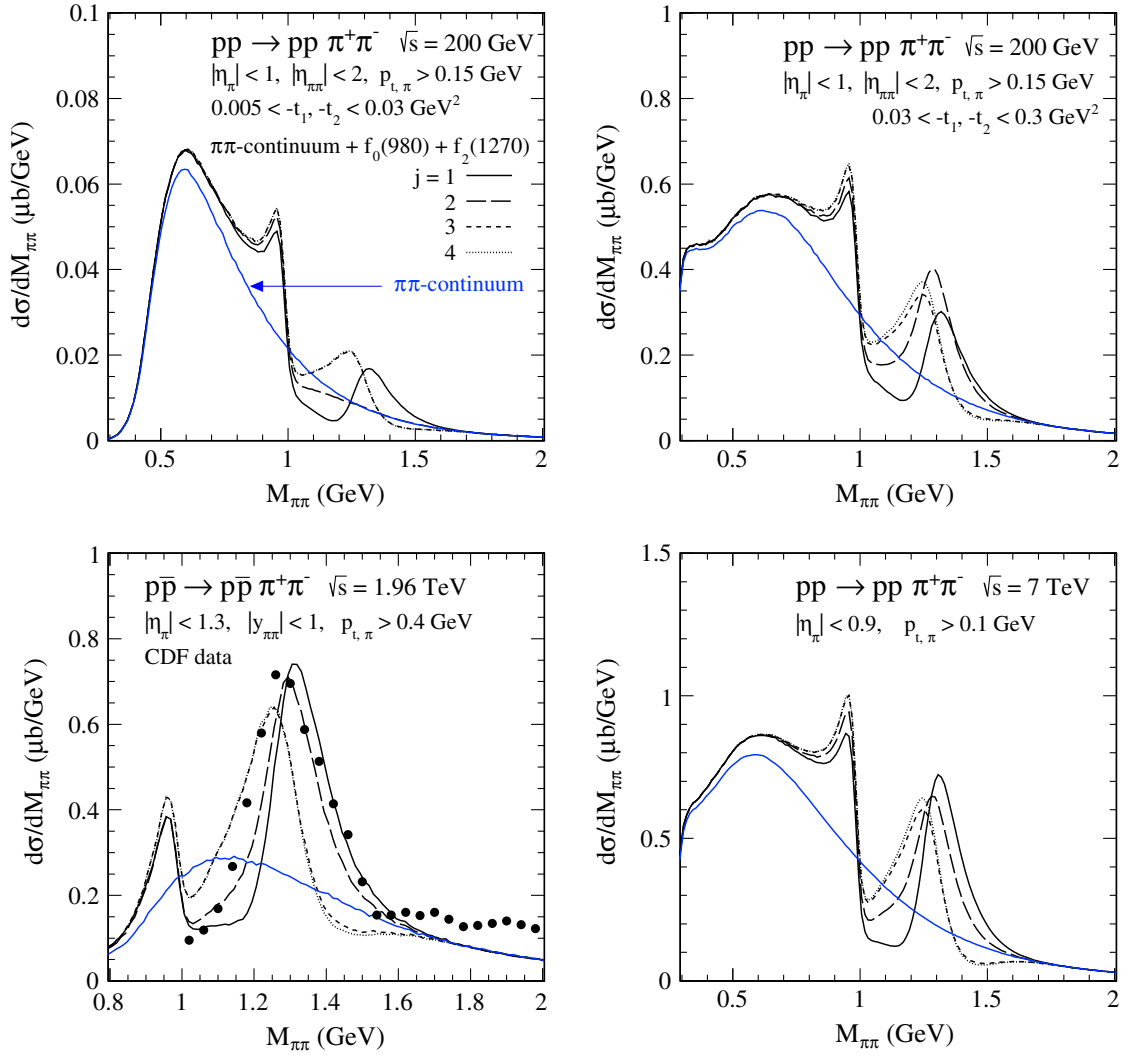
FIG. 9. Two-pion invariant mass distribution with the relevant experimental kinematical cuts specified in the legend. The results corresponding to the Born calculations were multiplied for $\sqrt{s} = 200$ GeV by the gap survival factor $\langle S^2 \rangle = 0.2$ and by $\langle S^2 \rangle = 0.1$ for $\sqrt{s} = 1.96$ and 7 TeV. The CDF data from [6] are shown for comparison. The blue solid lines represent the nonresonant continuum contribution obtained for the monopole off-shell pion form factors (3.18) with $\Lambda_{\text{off},M} = 0.7$ GeV. The black lines represent a coherent sum of the nonresonant continuum, $f_0(980)$ and $f_2(1270)$ resonant terms. The individual contributions of different $\mathbb{PP}f_2$ couplings $j = 1$ (the solid line), $j = 2$ (the long-dashed line), $j = 3$ (the dashed line), $j = 4$ (the dotted line) are shown. The results have been obtained with the coupling constant parameters: $g'_{\mathbb{PP}f_0(980)} = 0.2$, $g''_{\mathbb{PP}f_0(980)} = 1.0$, $g^{(1)}_{\mathbb{PP}f_2} = 2.0$, $g^{(2)}_{\mathbb{PP}f_2} = 9.0$, $g^{(3)}_{\mathbb{PP}f_2} = 0.5$, and $g^{(4)}_{\mathbb{PP}f_2} = 2.0$.

dipion invariant mass distribution observed by different experiments assuming only one $\mathbb{PP}f_2$ tensorial coupling. The calculations were done at Born level and the absorption corrections were taken into account by multiplying the cross section for the corresponding collision energy by a common factor $\langle S^2 \rangle$ obtained from [16]. The two-pion continuum was fixed by choosing as a parameter of the form factor for off-shell pion $\Lambda_{\text{off},M} = 0.7$ GeV; see (3.18). In addition, we include the $f_0(980)$ contribution where we chose the $\mathbb{PP}f_0(980)$ coupling parameters as $g'_{\mathbb{PP}f_0(980)} = 0.2$ and

$g''_{\mathbb{PP}f_0(980)} = 1.0$.[6] For each choice of the $\mathbb{PP}f_2$ coupling defined by the index j, we have adjusted the corresponding coupling constant to get the same cross section in the maximum corresponding to the $f_2(1270)$ resonance in the CDF data [6]. We assume that the peak

---

[6]Note that we take here smaller values of the coupling parameters than in our previous paper [19] because they were fixed there at the WA102 energy where we expect also large contributions to the cross section from the Reggeon exchanges.
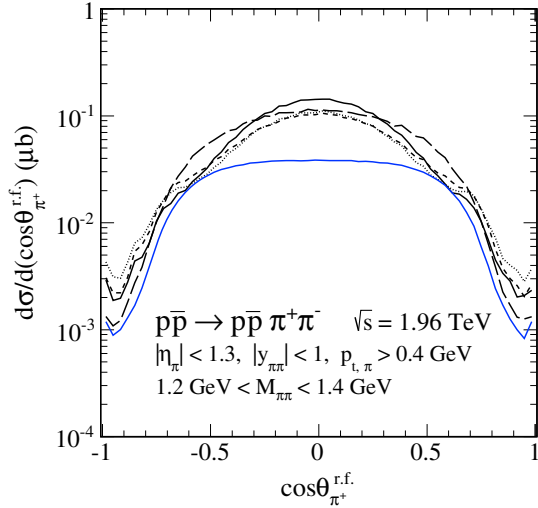
FIG. 10. Differential cross section $d\sigma/d(\cos\theta_{\pi^+}^{r.f.})$ as a function of the cosine of the polar angle $\theta_{\pi^+}^{r.f.}$ in the $\pi^+\pi^-$ rest frame for $\sqrt{s} = 1.96$ TeV and in the mass region $1.2\,\text{GeV} \leq M_{\pi\pi} \leq 1.4\,\text{GeV}$. The meaning of the lines is the same as in Fig. 9. Both signal ($f_2(1270)$) and background are included here.

observed experimentally corresponds mainly to the f_2 resonance.[7] As can be clearly seen from Fig. 9, different couplings generate different interference patterns. We can observe that the $j = 2$ coupling gives results close to those observed by the CDF Collaboration [6,7]. In this preliminary study, we do not try to fit the existing data by mixing different couplings because the CDF data are not fully exclusive (the outgoing p and $\bar{p}$ were not measured). Comparing the two upper panels ($\sqrt{s} = 200$ GeV) we see again that, for $j = 2$ (the long-dashed line), the f_2 is practically absent at small $|t_{1,2}|$ but is prominent at large $|t_{1,2}|$. In the calculation for the CDF kinematics, the results of which are shown in the bottom-left panel of Fig. 9, the ratio of the $f_2(1270)$ resonance signal at the resonance position to the corresponding value of the background contribution is about a factor of 2. In general, the ratio depends strongly on the kinematical conditions.

In Fig. 10, the $\cos\theta_{\pi^+}^{r.f.}$ distribution is shown in the f_2 mass region 1.2 GeV $\leq M_{\pi\pi} \leq 1.4$ GeV with the CDF kinematical cuts. The limited CDF acceptance, in particular $p_{t,\pi} > 0.4$ GeV, cause that differences for the different couplings are now less pronounced. Whether it is possible to pin down the correct couplings may require detailed studies of the CDF data; see [7]. We expect that these differences should be better visible in future LHC experiments.

In Figs. 11 and 12, we show the $\pi^+\pi^-$ invariant mass distribution for the STAR, ALICE and CMS experiments, respectively. The experimental data on central exclusive $\pi^+\pi^-$ production measured at the energies of the ISR, RHIC, and the LHC collider all show a broad continuum in the $\pi^+\pi^-$ invariant mass region of $M_{\pi\pi} < 1$ GeV. This region is experimentally difficult to access due to the missing acceptance for pion pairs and low pion transverse momentum. In addition, this region of the phase space may be affected by $\pi\pi$ final state interaction which may occur in addition to the direct coupling of Pomerons to $f_0(500)$ meson considered here.[8] Therefore, we show here results including, in addition to the nonresonant $\pi^+\pi^-$ continuum, the $f_2(1270)$ and the $f_0(980)$, the contribution from photoproduction, both resonant ($\rho^0 \to \pi^+\pi^-$) and nonresonant (Drell-Söding), and the $f_0(500)$ contribution.[9] The complete results for two values of coupling constant, $g'_{\mathbb{PP}f_0(500)} = 0.2$ and 0.5 correspond to the black long-dashed and solid lines, respectively. For comparison, we show also the contributions of the individual terms separately. The red solid lines represent the results for the $\pi^+\pi^-$-photoproduction contribution as obtained in [22], where both the resonant ($\rho(770)$, $\rho(1450)$) and the nonresonant (Drell-Söding) terms were included. The blue long-dashed (solid) lines are the results for the purely diffractive $\pi^+\pi^-$ production with $g'_{\mathbb{PP}f_0(500)} = 0.2$ (0.5) and the other parameters as specified in the caption of Fig. 11. The absorption effects lead to huge damping of the cross section for the purely diffractive term and relatively small reduction of the cross section for the photoproduction term. Therefore we expect one could observe the photoproduction term, especially at higher energies.

In Fig. 12, we show very recent results obtained by the CMS Collaboration. This measurement [11] is not fully exclusive, and the $M_{\pi\pi}$ spectrum contains therefore contributions associated with one or both protons undergoing dissociation. In the left panel, we show results obtained with the parameter set used to "describe" STAR [4] and CDF [6] data. At present, we cannot decide whether the disagreement is due to a large dissociation contribution in the CMS data [11] or due to an inappropriate parameter set. Therefore, in the right panel, we show results with parameters better adjusted to the new CMS data. If we used this set for STAR or CDF measurements our results there would be above the preliminary STAR data [4] at $M_{\pi\pi} > 1$ GeV and in complete disagreement with the CDF data from [6]; see Figs. 9 and 11. Only purely central exclusive data

---

[7]In principle, there may also be a contribution from the broad scalar $f_0(1370)$.

[8]The low-energy $\pi\pi$ final state interaction was discussed e.g. in [12,43–45].

[9]We have checked numerically that the interference effect between the two classes of processes, diffractive and photoproduction, is always below 1%.
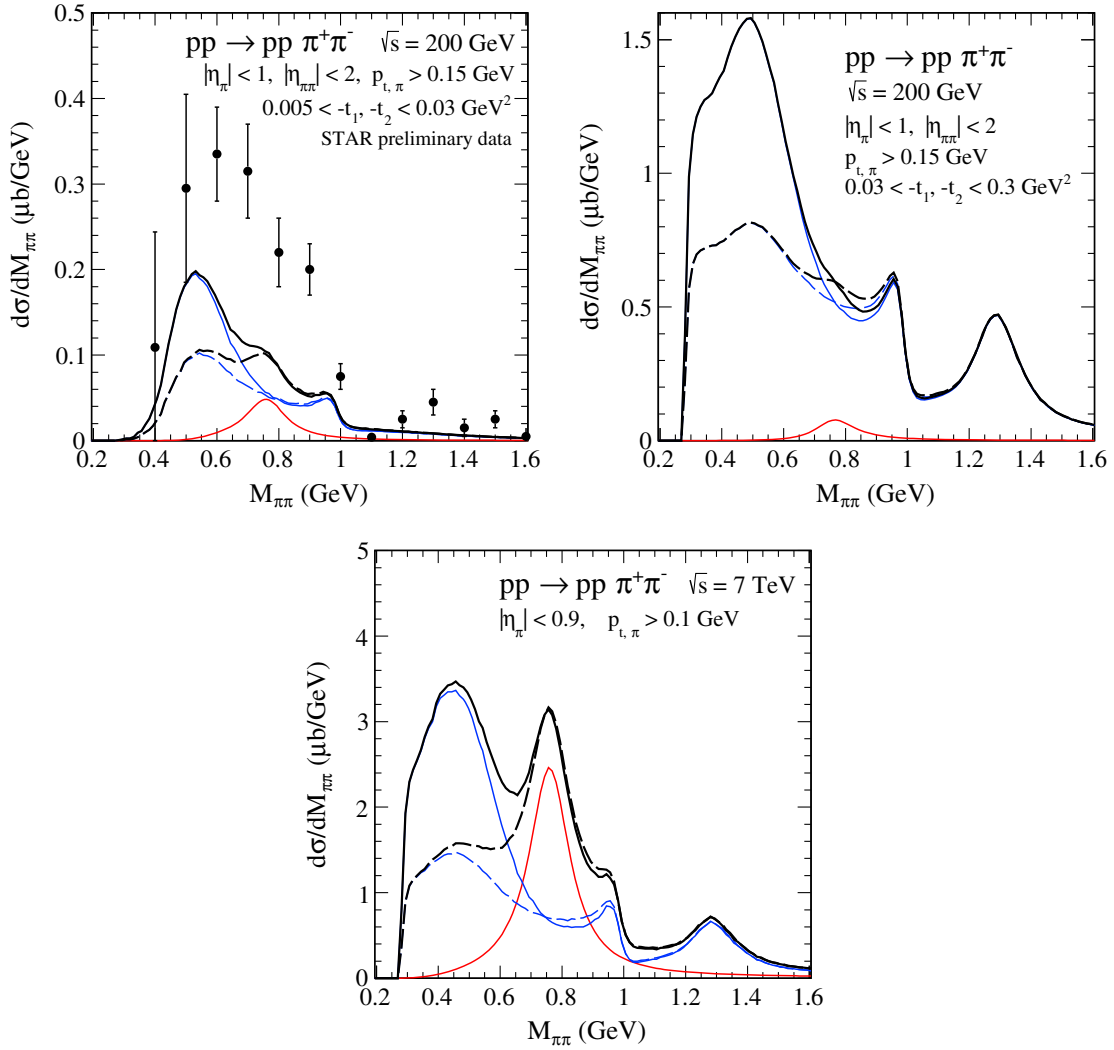
FIG. 11.   Two-pion invariant mass distribution for different experimental kinematical cuts. The results corresponding to the Born calculations for $\sqrt{s} = 200$ GeV and $\sqrt{s} = 7$ TeV were multiplied by the gap survival factors $\langle S^2 \rangle = 0.2$ and $\langle S^2 \rangle = 0.1$, respectively. The STAR [4] preliminary data are shown for comparison. The red solid lines represent results for the photoproduction contribution with $\langle S^2 \rangle = 0.9$. The blue solid and long-dashed lines represent the coherent sum of the purely diffractive production terms, that is, the continuum, $f_0(500)$, $f_0(980)$, and $f_2(1270)$ contributions. The complete results for $g'_{\mathbb{PP}f_0(500)} = 0.2$ and 0.5 ($g''_{\mathbb{PP}f_0(500)} = 0$ in (4.11)) correspond to the black long-dashed line and the solid line, respectively. The other parameters were chosen as $\Lambda_{\text{off},M} = 0.7$ GeV, $g'_{\mathbb{PP}f_0(980)} = 0.2$, $g''_{\mathbb{PP}f_0(980)} = 1.0$, and $g^{(2)}_{\mathbb{PP}f_2} = 9.0$.

expected from CMS-TOTEM and ATLAS-ALFA will allow us to draw definite conclusions.

The dipion invariant mass spectrum depends on cuts and/or selection conditions. As an example, we show in Fig. 13 the $M_{\pi\pi}$ distribution for the ALICE kinematics at $\sqrt{s} = 7$ TeV and with extra restrictions on azimuthal angle between the outgoing pions (the left panel) and with restrictions on transverse momentum of the pion pair (the right panel). Here we use again only the $j = 2$ coupling for $g_{\mathbb{PP}f_2}$. In the left panel, the complete results, including all interference terms, are shown as black full (for $\phi_{\pi\pi} > \pi/2$) and black long-dashed (for $\phi_{\pi\pi} < \pi/2$)

lines. We show the contributions from photoproduction (red line) and diffractive production (blue line) separately. In the right panel, the red and blue lines have the same meaning with the full and long-dashed lines corresponding to $p_{t,\pi\pi} > 0.5$ GeV and $p_{t,\pi\pi} < 0.5$ GeV, respectively. If we impose a $\phi_{\pi\pi} > \pi/2$ cut, we can see that the ρ^0 and f_2 resonance contributions are strongly enhanced. Two-dimensional correlations between the variables $p_{t,\pi}$, $p_{t,\pi\pi}$, $\phi_{\pi\pi}$, $\cos\theta^{r.f}_{\pi^+}$, and $M_{\pi\pi}$ are displayed in Fig. 14 for $\sqrt{s} = 7$ TeV. We predict complex and interesting patterns which could be checked by the ALICE Collaboration.
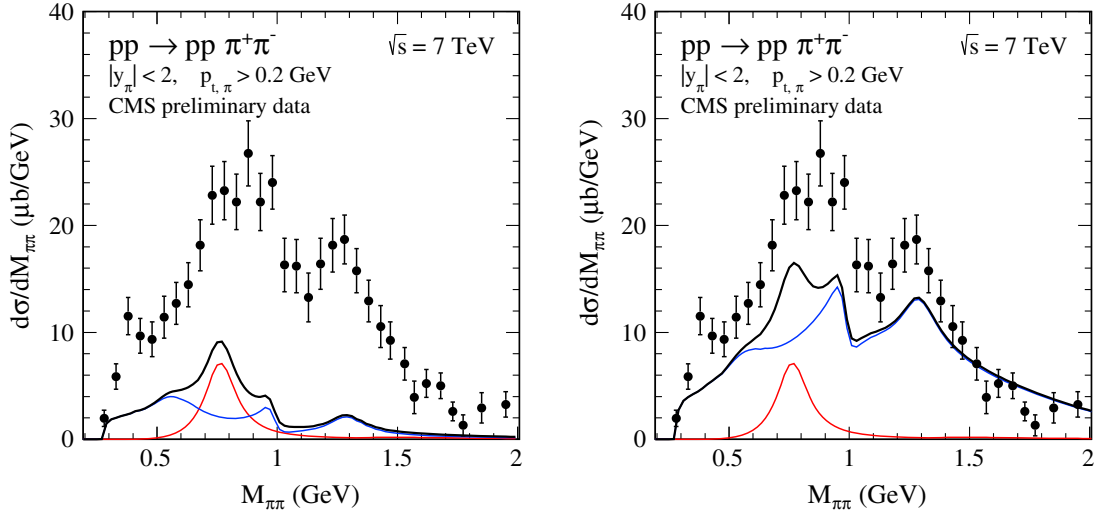
FIG. 12.   Two-pion invariant mass distribution for the CMS kinematics at $\sqrt{s} = 7$ TeV. The meaning of the lines is the same as in Fig. 11. Both photoproduction and purely diffractive contributions are included here. The complete results correspond to the black solid line. The CMS preliminary data [11] are shown for comparison. In the left panel, we show results for the standard parameter set as specified in the caption of Fig. 11. In the right panel, we take $\Lambda_{\text{off},E} = 1.6$ GeV in (3.17), $g'_{\mathbb{P}\mathbb{P}f_0(500)} = 0.5$, $g'_{\mathbb{P}\mathbb{P}f_0(980)} = 0.2$, $g''_{\mathbb{P}\mathbb{P}f_0(980)} = 1.0$, and $g^{(2)}_{\mathbb{P}\mathbb{P}f_2} = 15.0$.
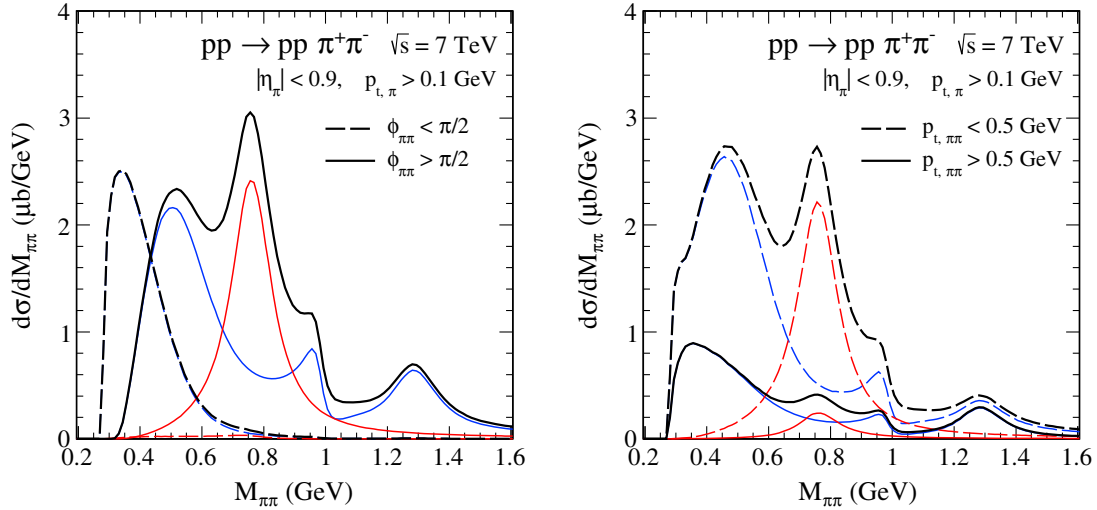

FIG. 13.   Two-pion invariant mass distribution for different experimental kinematical cuts for $\sqrt{s} = 7$ TeV. We show distributions with extra restrictions on azimuthal angle between the outgoing pions $\phi_{\pi\pi}$ (the left panel) and on transverse momentum of the pion pair (the right panel). The red solid lines represent results for the photoproduction contribution with $\langle S^2 \rangle = 0.9$. The blue lines represent the coherent sum of the continuum, $f_0(500)$, $f_0(980)$ and $f_2(1270)$ contributions with the same set of parameters as in Fig. 11 (we take here $g'_{\mathbb{P}\mathbb{P}f_0(500)} = 0.5$ and $\langle S^2 \rangle = 0.1$). The complete results correspond to the black solid and long-dashed lines, respectively.

VI. CONCLUSIONS

In the present paper, we have concentrated on the exclusive production of the tensor meson $f_2(1270)$ and the dipion continuum in central diffractive production via "fusion" of two tensor Pomerons. We have presented for the first time the corresponding amplitudes at Born level.

In the case of a tensor meson and tensor Pomerons, we have written down all (seven) possible Pomeron-Pomeron–f_2 couplings (vertices) and the corresponding amplitudes using the effective-field-theoretical approach proposed in [18]. The corresponding coupling constants in such a model are, however, unknown. In the future,
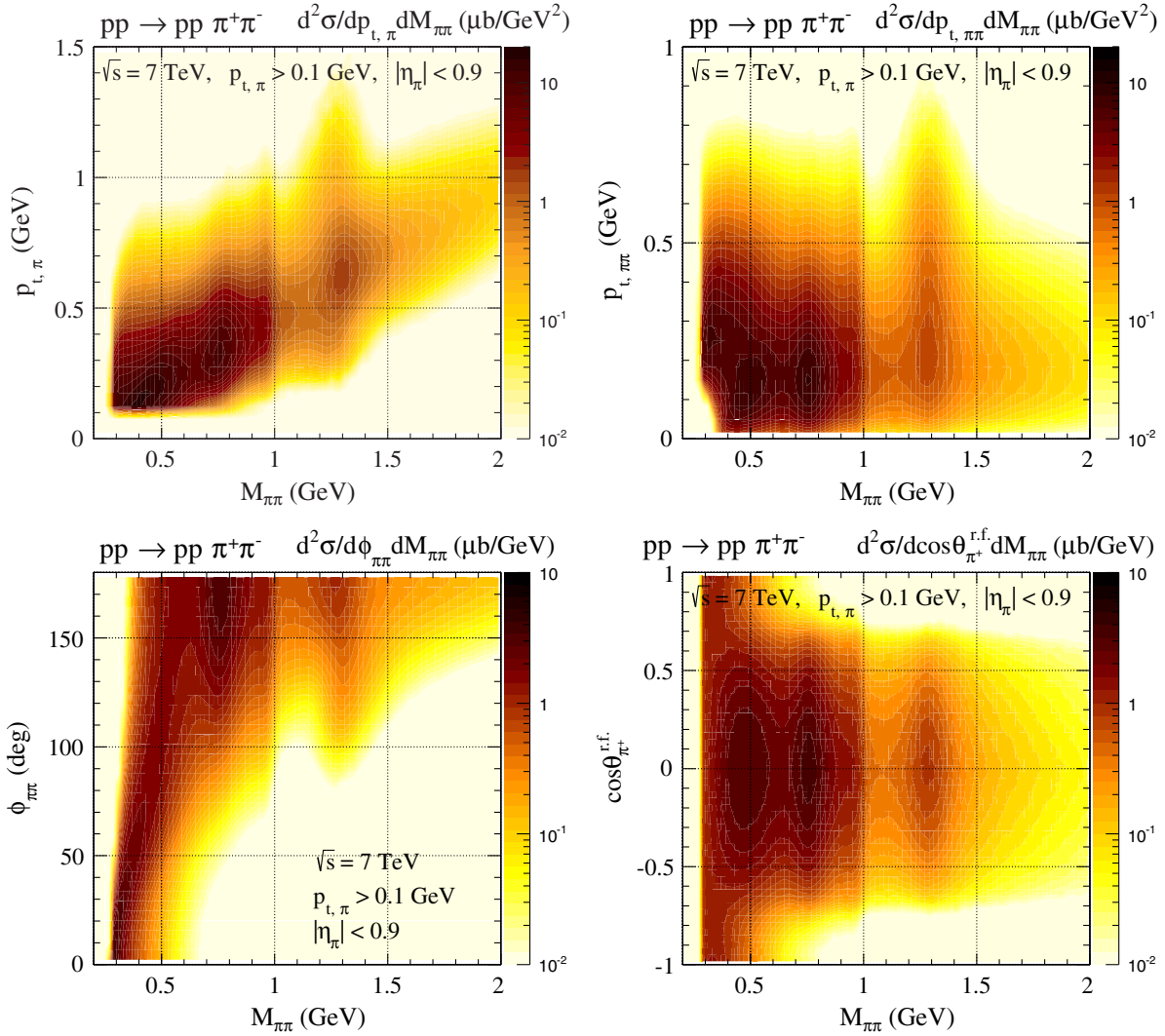
FIG. 14. The distributions for the ALICE kinematics at $\sqrt{s} = 7$ TeV. Plotted is $\frac{d^2\sigma}{dp_{t,\pi}dM_{\pi\pi}}$ (the top left panel), $\frac{d^2\sigma}{dp_{t,\pi\pi}dM_{\pi\pi}}$ (the top right panel), $\frac{d^2\sigma}{d\phi_{\pi\pi}dM_{\pi\pi}}$ (the bottom left panel), and $\frac{d^2\sigma}{d\cos\theta_{\pi^+}^{r.f.}dM_{\pi\pi}}$ (the bottom right panel). Both the purely diffractive (the nonresonant and resonant $f_0(500)$, $f_0(980)$, $f_2(1270)$ production) and the photoproduction (the Drell-Söding and resonant $\rho(770)$ production) processes were included in the calculations. Here, the model parameters were chosen as in Fig. 11. Absorption corrections were taken into account effectively by the gap survival factors $\langle S^2 \rangle = 0.1$ and 0.9 for the fully diffractive and photoproduction contributions, respectively.

they could be adjusted by comparison with precise experimental data.

Here we have tried to see whether one of the Pomeron-Pomeron–f_2 couplings (tensorial structures) could be sufficient. Thus we have tried to adjust only one coupling constant at the time to the cross section at the resonance maximum. The different couplings (tensorial structures) give different results due to different interference effects of the resonance and the dipion continuum. By assuming dominance of one of the couplings, we can get only a rough description of the recent CDF and preliminary STAR experimental data. The model parameters of the optimal coupling ($j = 2$) have been roughly adjusted to recent CDF data and then used for the predictions for the STAR,

ALICE, and CMS experiments.[10] For experimental analyses of future data, the ratio of resonance contributions to the background may be of practical importance. We have found, for example, that for the CDF experimental conditions, the f_2-to-background ratio is about a factor of 2. We have also included the scalar $f_0(500)$ and $f_0(980)$ resonances, and the vector $\rho(770)$ resonance in a consistent

---

[10] A better adjustment of the model parameters, including more than one Pomeron-Pomeron–f_2 coupling will be possible with better experimental data which are expected soon. Then a corresponding Monte Carlo generator could be constructed. At present, most of the existing Monte Carlo codes [46,47] include only the purely diffractive $\pi^+\pi^-$ continuum (for an exception, see [48]).

way. We have shown that the resonance structures in the measured two-pion invariant mass spectra depend on the cut on proton transverse momenta and/or on four-momentum transfer squared $t_{1,2}$ used in an experiment. The cuts may play then the role of a $\pi\pi$ resonance filter. We have presented several interesting correlation distributions which could be checked by the experiments.

To summarize, we have given a consistent treatment of the $\pi^+\pi^-$ continuum and resonance production in central exclusive pp and $p\bar{p}$ collisions in an effective field-theoretic approach. A rich structure emerged which should give experimentalists interesting challenges to check and explore. In this way, we shall gain insight into how two Pomerons couple to tensor mesons like the $f_2(1270)$. Assuming this will be clarified in future experiments, we then have the big theory challenge of deriving such couplings from basic QCD.

ACKNOWLEDGMENTS

APPENDIX A: $\mathbb{P}\mathbb{P}f_2$ COUPLINGS

Here we discuss the couplings $\mathbb{P}\mathbb{P}f_2$. Consider first the fictitious fusion reaction of two "tensor-Pomeron particles" giving the f_2 state; see Appendix A of [19]. From Table VI of [19], we find that the following values of

(l, S) can lead to the f_2 state, a $J^{PC} = 2^{++}$ meson: $(l, S) = (0, 2), (2,0), (2,2), (2,4), (4,2), (4,4), (6,4)$. Thus, we should be able to construct seven independent coupling Lagrangians $\mathbb{P}\mathbb{P}f_2$:

$$\mathcal{L}'(x) = \sum_{j=1}^{7} \mathcal{L}'^{(j)}(x). \tag{A1}$$

In order to write the corresponding formulas in a compact and convenient form, we find it useful to define the tensor

$$R_{\mu\nu\kappa\lambda} = \frac{1}{2} g_{\mu\kappa} g_{\nu\lambda} + \frac{1}{2} g_{\mu\lambda} g_{\nu\kappa} - \frac{1}{4} g_{\mu\nu} g_{\kappa\lambda}, \tag{A2}$$

which fulfils the following relations:

$$R_{\mu\nu\kappa\lambda} = R_{\nu\mu\kappa\lambda} = R_{\mu\nu\lambda\kappa} = R_{\kappa\lambda\mu\nu},$$
$$R_{\mu\nu\kappa\lambda} g^{\kappa\lambda} = 0, \qquad R_{\mu\nu\kappa\lambda} R^{\kappa\lambda}{}_{\rho\sigma} = R_{\mu\nu\rho\sigma},$$
$$R_{\mu\nu\rho_1\alpha} R_{\kappa\lambda\sigma_1}{}^{\alpha} R_{\rho\sigma}{}^{\rho_1\sigma_1} = R_{\mu\nu\mu_1\nu_1} R_{\kappa\lambda\alpha_1\lambda_1} R_{\rho\sigma\rho_1\sigma_1} g^{\nu_1\alpha_1} g^{\lambda_1\rho_1} g^{\sigma_1\mu_1}. \tag{A3}$$

For every tensor $T_{\alpha\beta}$ with $T_{\alpha\beta} = T_{\beta\alpha}$ and $T_{\alpha\beta} g^{\alpha\beta} = 0$, we have

$$R_{\kappa\lambda\alpha\beta} T^{\alpha\beta} = T_{\kappa\lambda}. \tag{A4}$$

Now we write down the coupling Lagrangians. In the following, $\mathbb{P}_{\mu\nu}(x)$ and $\phi_{\rho\sigma}(x)$ are the effective tensor-Pomeron and f_2 field operators, respectively. We define

$$\mathcal{L}'^{(1)}(x) = M_0 g^{(1)}_{\mathbb{P}\mathbb{P}f_2} \mathbb{P}_{\mu_1\nu_1}(x) \mathbb{P}_{\alpha_1\lambda_1}(x) \phi_{\rho_1\sigma_1}(x) R^{\mu_1\nu_1\mu_2\nu_2} R^{\alpha_1\lambda_1\alpha_2\lambda_2} R^{\rho_1\sigma_1\rho_2\sigma_2} g_{\nu_2\alpha_2} g_{\lambda_2\rho_2} g_{\sigma_2\mu_2}, \tag{A5}$$

$$\mathcal{L}'^{(2)}(x) = \frac{1}{M_0} g^{(2)}_{\mathbb{P}\mathbb{P}f_2} (\partial_\mu \mathbb{P}_{\kappa\alpha}(x) - \partial_\kappa \mathbb{P}_{\mu\alpha}(x))(\partial_\nu \mathbb{P}_{\lambda\beta}(x) - \partial_\lambda \mathbb{P}_{\nu\beta}(x)) g^{\alpha\beta} g^{\mu\nu} R^{\kappa\lambda\rho\sigma} \phi_{\rho\sigma}(x), \tag{A6}$$

$$\mathcal{L}'^{(3)}(x) = \frac{1}{M_0} g^{(3)}_{\mathbb{P}\mathbb{P}f_2} (\partial_\mu \mathbb{P}_{\kappa\alpha}(x) + \partial_\kappa \mathbb{P}_{\mu\alpha}(x))(\partial_\nu \mathbb{P}_{\lambda\beta}(x) + \partial_\lambda \mathbb{P}_{\nu\beta}(x)) g^{\alpha\beta} g^{\mu\nu} R^{\kappa\lambda\rho\sigma} \phi_{\rho\sigma}(x), \tag{A7}$$

$$\mathcal{L}'^{(4)}(x) = \frac{1}{M_0} g^{(4)}_{\mathbb{P}\mathbb{P}f_2} (\partial^\kappa \mathbb{P}_{\mu\nu}(x))(\partial^\mu \mathbb{P}_{\kappa\lambda}(x)) \phi^{\nu\lambda}(x), \tag{A8}$$

$$\mathcal{L}'^{(5)}(x) = \frac{1}{M_0^3} g^{(5)}_{\mathbb{P}\mathbb{P}f_2} [\partial_\kappa (\partial_\mu \mathbb{P}_{\nu\alpha}(x) - \partial_\nu \mathbb{P}_{\mu\alpha}(x))][\partial_\lambda (\partial^\mu \mathbb{P}^{\nu\alpha}(x) - \partial^\nu \mathbb{P}^{\mu\alpha}(x))] \phi^{\kappa\lambda}(x), \tag{A9}$$

$$\mathcal{L}'^{(6)}(x) = \frac{1}{M_0^3} g^{(6)}_{\mathbb{P}\mathbb{P}f_2} (\partial^\kappa \partial^\lambda \mathbb{P}_{\mu\nu}(x))(\partial^\mu \partial_\rho \mathbb{P}_{\kappa\lambda}(x)) \phi^{\nu\rho}(x), \tag{A10}$$

$$\mathcal{L}'^{(7)}(x) = \frac{1}{M_0^5} g^{(7)}_{\mathbb{P}\mathbb{P}f_2} (\partial^\rho \partial^\kappa \partial^\lambda \mathbb{P}_{\mu\nu}(x))(\partial^\sigma \partial^\mu \partial^\nu \mathbb{P}_{\kappa\lambda}(x)) \phi_{\rho\sigma}(x). \tag{A11}$$

In (A5) to (A11), $M_0 \equiv 1$ GeV and the $g^{(j)}_{\mathbb{P}\mathbb{P}f_2}$ are dimensionless coupling constants. The values of coupling constants $g^{(j)}_{\mathbb{P}\mathbb{P}f_2}$, where $j = 1, \ldots, 7$, of nonperturbative origin, are not known and are not easy to find from first principles.

The vertices as obtained from (A5) to (A11) with the momentum and Lorentz-indices assignments shown in Fig. 15 are as follows:

$$i\Gamma^{(\mathbb{P}\mathbb{P}f_2)(1)}_{\mu\nu,\kappa\lambda,\rho\sigma} = 2ig^{(1)}_{\mathbb{P}\mathbb{P}f_2}M_0 R_{\mu\nu\mu_1\nu_1}R_{\kappa\lambda\alpha_1\lambda_1}R_{\rho\sigma\rho_1\sigma_1}g^{\nu_1\alpha_1}g^{\lambda_1\rho_1}g^{\sigma_1\mu_1}, \tag{A12}$$

$$i\Gamma^{(\mathbb{P}\mathbb{P}f_2)(2)}_{\mu\nu,\kappa\lambda,\rho\sigma}(q_1,q_2) = -\frac{2i}{M_0}g^{(2)}_{\mathbb{P}\mathbb{P}f_2}((q_1 \cdot q_2)R_{\mu\nu\rho_1\alpha}R_{\kappa\lambda\sigma_1}{}^{\alpha} - q_{1\rho_1}q_2^{\mu_1}R_{\mu\nu\mu_1\alpha}R_{\kappa\lambda\sigma_1}{}^{\alpha} - q_1^{\mu_1}q_{2\sigma_1}R_{\mu\nu\rho_1\alpha}R_{\kappa\lambda\mu_1}{}^{\alpha} + q_{1\rho_1}q_{2\sigma_1}R_{\mu\nu\kappa\lambda})R_{\rho\sigma}{}^{\rho_1\sigma_1}, \tag{A13}$$

$$i\Gamma^{(\mathbb{P}\mathbb{P}f_2)(3)}_{\mu\nu,\kappa\lambda,\rho\sigma}(q_1,q_2) = -\frac{2i}{M_0}g^{(3)}_{\mathbb{P}\mathbb{P}f_2}((q_1 \cdot q_2)R_{\mu\nu\rho_1\alpha}R_{\kappa\lambda\sigma_1}{}^{\alpha} + q_{1\rho_1}q_2^{\mu_1}R_{\mu\nu\mu_1\alpha}R_{\kappa\lambda\sigma_1}{}^{\alpha} + q_1^{\mu_1}q_{2\sigma_1}R_{\mu\nu\rho_1\alpha}R_{\kappa\lambda\mu_1}{}^{\alpha} + q_{1\rho_1}q_{2\sigma_1}R_{\mu\nu\kappa\lambda})R_{\rho\sigma}{}^{\rho_1\sigma_1}, \tag{A14}$$

$$i\Gamma^{(\mathbb{P}\mathbb{P}f_2)(4)}_{\mu\nu,\kappa\lambda,\rho\sigma}(q_1,q_2) = -\frac{i}{M_0}g^{(4)}_{\mathbb{P}\mathbb{P}f_2}(q_1^{\alpha_1}q_2^{\mu_1}R_{\mu\nu\mu_1\nu_1}R_{\kappa\lambda\alpha_1\lambda_1} + q_2^{\alpha_1}q_1^{\mu_1}R_{\mu\nu\alpha_1\lambda_1}R_{\kappa\lambda\mu_1\nu_1})R^{\nu_1\lambda_1}{}_{\rho\sigma}, \tag{A15}$$

$$i\Gamma^{(\mathbb{P}\mathbb{P}f_2)(5)}_{\mu\nu,\kappa\lambda,\rho\sigma}(q_1,q_2) = -\frac{2i}{M_0^3}g^{(5)}_{\mathbb{P}\mathbb{P}f_2}(q_1^{\mu_1}q_2^{\nu_1}R_{\mu\nu\nu_1\alpha}R_{\kappa\lambda\mu_1}{}^{\alpha} + q_1^{\nu_1}q_2^{\mu_1}R_{\mu\nu\mu_1\alpha}R_{\kappa\lambda\nu_1}{}^{\alpha} - 2(q_1 \cdot q_2)R_{\mu\nu\kappa\lambda})q_{1\alpha_1}q_{2\lambda_1}R^{\alpha_1\lambda_1}{}_{\rho\sigma}, \tag{A16}$$

$$i\Gamma^{(\mathbb{P}\mathbb{P}f_2)(6)}_{\mu\nu,\kappa\lambda,\rho\sigma}(q_1,q_2) = \frac{i}{M_0^3}g^{(6)}_{\mathbb{P}\mathbb{P}f_2}(q_1^{\alpha_1}q_1^{\lambda_1}q_2^{\mu_1}q_{2\rho_1}R_{\mu\nu\mu_1\nu_1}R_{\kappa\lambda\alpha_1\lambda_1} + q_2^{\alpha_1}q_2^{\lambda_1}q_1^{\mu_1}q_{1\rho_1}R_{\mu\nu\alpha_1\lambda_1}R_{\kappa\lambda\mu_1\nu_1})R^{\nu_1\rho_1}{}_{\rho\sigma}, \tag{A17}$$

$$i\Gamma^{(\mathbb{P}\mathbb{P}f_2)(7)}_{\mu\nu,\kappa\lambda,\rho\sigma}(q_1,q_2) = -\frac{2i}{M_0^5}g^{(7)}_{\mathbb{P}\mathbb{P}f_2}q_1^{\rho_1}q_1^{\alpha_1}q_1^{\lambda_1}q_2^{\sigma_1}q_2^{\mu_1}q_2^{\nu_1}R_{\mu\nu\mu_1\nu_1}R_{\kappa\lambda\alpha_1\lambda_1}R_{\rho\sigma\rho_1\sigma_1}. \tag{A18}$$

From (A3) and (A12)–(A18), we have

$$g^{\mu\nu}\Gamma^{(\mathbb{P}\mathbb{P}f_2)(j)}_{\mu\nu,\kappa\lambda,\rho\sigma}(q_1,q_2) = 0, \qquad g^{\kappa\lambda}\Gamma^{(\mathbb{P}\mathbb{P}f_2)(j)}_{\mu\nu,\kappa\lambda,\rho\sigma}(q_1,q_2) = 0, \qquad g^{\rho\sigma}\Gamma^{(\mathbb{P}\mathbb{P}f_2)(j)}_{\mu\nu,\kappa\lambda,\rho\sigma}(q_1,q_2) = 0. \tag{A19}$$

The expressions (A12)–(A18) represent our bare vertices, which we use in (4.16) multiplied by a form factor.

Investigating the contributions of the vertices (A12) to (A18) to the fictitious reaction of two "real tensor Pomerons" annihilating to the f_2 meson, we find that we can associate the couplings $j = 1, \ldots, 7$ with the following (l, S) values: $(0,2), (2, 0)–(2, 2), (2, 0) + (2, 2), (2,4), (4,2), (4,4), (6,4)$, respectively.
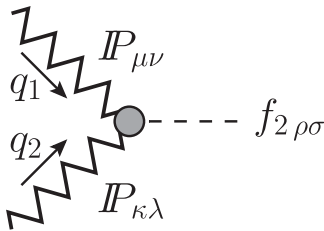

FIG. 15. Generic diagram for the $\mathbb{P}\mathbb{P}f_2$ vertices (A12)–(A18) with momentum and Lorentz-indices assignments.

APPENDIX B: ASYMMETRIES DUE TO INTERFERENCE OF DIFFERENT CHARGE-CONJUGATION EXCHANGES

Here we return to asymmetries generated by the interference of $(C_1, C_2) = (1, 1)$, that is, our purely diffractive continuum and resonance terms and the $(C_1, C_2) = (1, -1) + (-1, 1)$ terms from photoproduction; see Sec. III. In the $\pi^+\pi^-$ rest frame, we choose the Collins-Soper basis [39] with unit vectors

$$e_1 = \frac{\hat{p}_a + \hat{p}_b}{|\hat{p}_a + \hat{p}_b|},$$
$$e_2 = \frac{\hat{p}_a \times \hat{p}_b}{|\hat{p}_a \times \hat{p}_b|},$$
$$e_3 = \frac{\hat{p}_a - \hat{p}_b}{|\hat{p}_a - \hat{p}_b|}, \tag{B1}$$

where $\hat{p}_a = p_a/|p_a|$ and $\hat{p}_b = p_b/|p_b|$. We define in this frame the unit vector

$$\hat{\boldsymbol{k}} = \frac{\boldsymbol{p_3} - \boldsymbol{p_4}}{|\boldsymbol{p_3} - \boldsymbol{p_4}|} = \begin{pmatrix} \sin\chi\sin\psi \\ \cos\chi \\ \sin\chi\cos\psi \end{pmatrix},$$

$$0 \leq \chi \leq \pi, \qquad 0 \leq \psi < 2\pi. \qquad \text{(B2)}$$

We are interested in the distribution of the vector $\hat{\boldsymbol{k}}$. From parity invariance, which holds for strong and electromagnetic processes, we get that this distribution must be symmetric under $\hat{\boldsymbol{k}} \cdot \boldsymbol{e_2} \to -\hat{\boldsymbol{k}} \cdot \boldsymbol{e_2}$. That is, parity requires symmetry under the replacement

$$\cos\chi \to -\cos\chi$$
$$\psi \to \psi. \qquad \text{(B3)}$$

If only $(C_1, C_2) = (1,1) + (-1,-1)$ or $(C_1, C_2) = (1,-1) + (-1,1)$ amplitudes contribute, the distribution must be symmetric under $\hat{\boldsymbol{k}} \to -\hat{\boldsymbol{k}}$. Thus, an asymmetry under $\hat{\boldsymbol{k}} \to -\hat{\boldsymbol{k}}$ signals an interference of the $(C_1, C_2) = (1,1) + (-1,-1)$ and $(C_1, C_2) = (1,-1) + (-1,1)$ amplitudes. For $\cos\chi$ and ψ, the replacement $\hat{\boldsymbol{k}} \to -\hat{\boldsymbol{k}}$ means

$$\cos\chi \to -\cos\chi$$
$$\psi \to \pi + \psi. \qquad \text{(B4)}$$

[1] A. Austregesilo (COMPASS Collaboration), A partial-wave analysis of centrally produced two-pseudoscalar final states in pp reactions at COMPASS, in *Proceedings, 51st International Winter Meeting on Nuclear Physics* (Bormio 2013), arXiv:1306.6814.

[2] A. Austregesilo, Central Production of Two-Pseudoscalar Meson Systems at the COMPASS Experiment at CERN, Report No. CERN-THESIS-2014-190.

[3] C. Adolph *et al.*, Resonance Production and $\pi\pi$ S-wave in $\pi^- + p \to \pi^- \pi^- \pi^+ + p_{recoil}$ at 190 GeV/c, arXiv:1509.00992.

[4] L. Adamczyk, W. Guryn, and J. Turnau, Central exclusive production at RHIC, Int. J. Mod. Phys. A **29**, 1446010 (2014).

[5] R. Sikora, in Proceedings of Central Exclusive Production of meson pairs in proton-proton collisions at $\sqrt{s} = 200$ GeV in the STAR experiment at RHIC, XXIII Low-x Meeting, Sandomierz, Poland, 2015.

[6] T. A. Aaltonen *et al.* (CDF Collaboration), Measurement of central exclusive $\pi^+\pi^-$ production in $p\bar{p}$ collisions at $\sqrt{s} = 0.9$ and 1.96 TeV at CDF, Phys. Rev. D **91**, 091101 (2015).

[7] M. Albrow, J. Lewis, M. Żurek, A. Święch, D. Lontkovskyi, I. Makarenko, and J. S. Wilson, in Measurement of Central Exclusive Hadron Pair Production in CDF, http://www-cdf.fnal.gov/physics/new/qcd/GXG_14/webpage/.

[8] R. Schicker, Diffractive production of mesons, Eur. Phys. J. Web Conf. **81**, 01005 (2014).

[9] R. Staszewski, P. Lebiedowicz, M. Trzebiński, J. Chwastowski, and A. Szczurek, Exclusive $\pi^+\pi^-$ production at the LHC with forward proton tagging, Acta Phys. Pol. B **42**, 1861 (2011).

[10] K. Österberg, Potential of central exclusive production studies in high β^* runs at the LHC with CMS-TOTEM, Int. J. Mod. Phys. A **29**, 1446019 (2014).

[11] (CMS Collaboration), Measurement of exclusive $\pi^+\pi^-$ production in proton-proton collisions at $\sqrt{s} = 7$ TeV, Report No. CMS-PAS-FSQ-12-004.

[12] P. Lebiedowicz and A. Szczurek, Exclusive $pp \to pp\pi^+\pi^-$ reaction: From the threshold to LHC, Phys. Rev. D **81**, 036003 (2010).

[13] P. Lebiedowicz, R. Pasechnik, and A. Szczurek, Measurement of exclusive production of scalar χ_{c0} meson in proton-(anti)proton collisions via $\chi_{c0} \to \pi^+\pi^-$ decay, Phys. Lett. B **701**, 434 (2011).

[14] P. Lebiedowicz and A. Szczurek, $pp \to ppK^+K^-$ reaction at high energies, Phys. Rev. D **85**, 014026 (2012).

[15] P. Lebiedowicz and A. Szczurek, Exclusive $pp \to nn\pi^+\pi^+$ reaction at LHC and RHIC, Phys. Rev. D **83**, 076002 (2011).

[16] P. Lebiedowicz and A. Szczurek, Revised model of absorption corrections for the $pp \to pp\pi^+\pi^-$ process, Phys. Rev. D **92**, 054001 (2015).

[17] O. Nachtmann, Considerations concerning diffraction scattering in quantum chromodynamics, Ann. Phys. (N.Y.) **209**, 436 (1991).

[18] C. Ewerz, M. Maniatis, and O. Nachtmann, A Model for Soft High-Energy Scattering: Tensor Pomeron and Vector Odderon, Ann. Phys. (NY) **342**, 31 (2014).

[19] P. Lebiedowicz, O. Nachtmann, and A. Szczurek, Exclusive central diffractive production of scalar and pseudoscalar mesons; tensorial vs. vectorial pomeron, Ann. Phys. (N.Y.) **344**, 301 (2014).

[20] D. Barberis *et al.* (WA102 Collaboration), A study of pseudoscalar states produced centrally in pp interactions at 450 GeV/c, Phys. Lett. B **427**, 398 (1998).

[21] N. I. Kochelev, T. Morii, B. L. Reznik, and A. V. Vinnikov, The role of secondary Reggeons in central meson production, Eur. Phys. J. A **8**, 405 (2000).

[22] P. Lebiedowicz, O. Nachtmann, and A. Szczurek, ρ^0 and Drell-Söding contributions to central exclusive production of $\pi^+\pi^-$ pairs in proton-proton collisions at high energies, Phys. Rev. D **91**, 074023 (2015).

[23] A. Bolz, C. Ewerz, M. Maniatis, O. Nachtmann, M. Sauter, and A. Schöning, Photoproduction of $\pi^+\pi^-$ pairs in a model with tensor-pomeron and vector-odderon exchange, J. High Energy Phys. 01 (2015) 151.

[24] A. Szczurek and P. Lebiedowicz, Exclusive scalar $f_0(1500)$ meson production for energy ranges available at the GSI Facility for Antiproton and Ion Research (GSI-FAIR) and at the Japan Proton Accelerator Research Complex (J-PARC), Nucl. Phys. **A826,** 101 (2009).

[25] W. Ochs, The status of glueballs, J. Phys. G **40,** 043001 (2013).

[26] T. Armstrong *et al.* (WA76 Collaboration), Study of the centrally produced $\pi\pi$ and $K\bar{K}$ systems at 85 GeV/c and 300 GeV/c, Z. Phys. C **51,** 351 (1991).

[27] D. Barberis *et al.* (WA102 Collaboration), A coupled channel analysis of the centrally produced K^+K^- and $\pi^+\pi^-$ final states in pp interactions at 450 GeV/c, Phys. Lett. B **462,** 462 (1999).

[28] D. Barberis *et al.* (WA102 Collaboration), A partial wave analysis of the centrally produced $\pi^+\pi^-$ system in pp interactions at 450 GeV/c, Phys. Lett. B **453,** 316 (1999).

[29] A. Kirk, Resonance production in central pp collisions at the CERN Omega spectrometer, Phys. Lett. B **489,** 29 (2000).

[30] A. Kirk, A review of central production experiments at the CERN Omega spectrometer, Int. J. Mod. Phys. A **29,** 1446001 (2014).

[31] D. Barberis *et al.* (WA102 Collaboration), A kinematical selection of glueball candidates in central production, Phys. Lett. B **397,** 339 (1997).

[32] A. Breakstone *et al.* (ABCDHW Collaboration), Production of the f^0 Meson in the Double Pomeron Exchange Reaction $pp \to pp\pi^+\pi^-$ at $\sqrt{s} = 62$ GeV, Z. Phys. C **31,** 185 (1986).

[33] A. Breakstone *et al.* (ABCDHW Collaboration), Inclusive Pomeron-Pomeron interactions at the CERN ISR, Z. Phys. C **42,** 387 (1989).

[34] A. Breakstone *et al.* (ABCDHW Collaboration), The reaction Pomeron-Pomeron $\to \pi^+\pi^-$ and an unusual production mechanism for the $f_2(1270)$, Z. Phys. C **48,** 569 (1990).

[35] T. Åkesson *et al.* (AFS Collaboration), A search for glueballs and a study of double pomeron exchange at the CERN intersecting storage rings, Nucl. Phys. **B264,** 154 (1986).

[36] V. A. Petrov, R. A. Ryutin, A. E. Sobol, and J.-P. Guillaud, Azimuthal angular distributions in EDDE as spin-parity analyser and glueball filter for LHC, J. High Energy Phys. 06 (2005) 007.

[37] R. Fiore, L. Jenkovszky, and R. Schicker, Resonance production in Pomeron-Pomeron collisions at the LHC, Eur. Phys. J. C **76,** 38 (2016).

[38] G. P. Lepage, Vegas: An Adaptive Multidimensional Integration Program, Report No. CLNS-80/447.

[39] J. C. Collins and D. E. Soper, Angular Distribution of Dileptons in High-Energy Hadron Collisions, Phys. Rev. D **16,** 2219 (1977).

[40] E. Byckling and K. Kajantie, *Particle Kinematics* (Wiley, London, 1973).

[41] A. Donnachie, H. G. Dosch, P. V. Landshoff, and O. Nachtmann, *Pomeron Physics and QCD* (Cambridge University Press, Cambridge, U.K., 2002), p. 1.

[42] K. A. Olive *et al.* (Particle Data Group), Review of Particle Physics, Chin. Phys. C **38,** 090001 (2014).

[43] J. Pumplin and F. S. Henyey, Double pomeron exchange in the reaction $pp \to pp\pi^+\pi^-$, Nucl. Phys. **B117,** 377 (1976).

[44] K. L. Au, D. Morgan, and M. R. Pennington, Meson dynamics beyond the quark model: Study of final-state interactions, Phys. Rev. D **35,** 1633 (1987).

[45] P. Lebiedowicz, A. Szczurek, and R. Kamiński, Low-energy pion-pion scattering in the $pp \to pp\pi^+\pi^-$ and $p\bar{p} \to p\bar{p}\pi^+\pi^-$ reactions, Phys. Lett. B **680,** 459 (2009).

[46] L. A. Harland-Lang, V. A. Khoze, and M. G. Ryskin, Modelling exclusive meson pair production at hadron colliders, Eur. Phys. J. C **74,** 2848 (2014).

[47] R. A. Kycia, J. Chwastowski, R. Staszewski, and J. Turnau, GenEx: A simple generator structure for exclusive processes in high energy collisions, arXiv:1411.6035.

[48] V. A. Petrov, R. A. Ryutin, A. E. Sobol, and J.-P. Guillaud, EDDE Monte Carlo event generator. Version 2.1, arXiv:0711.1794.